



Engineering
PERIODICALS
U 5000

University of Glasgow
DEPARTMENT OF
**AEROSPACE
ENGINEERING**

Calculation of the Flow Field around a Square
Section Cylinder undergoing Forced Transverse
Oscillations using a Discrete Vortex Method.

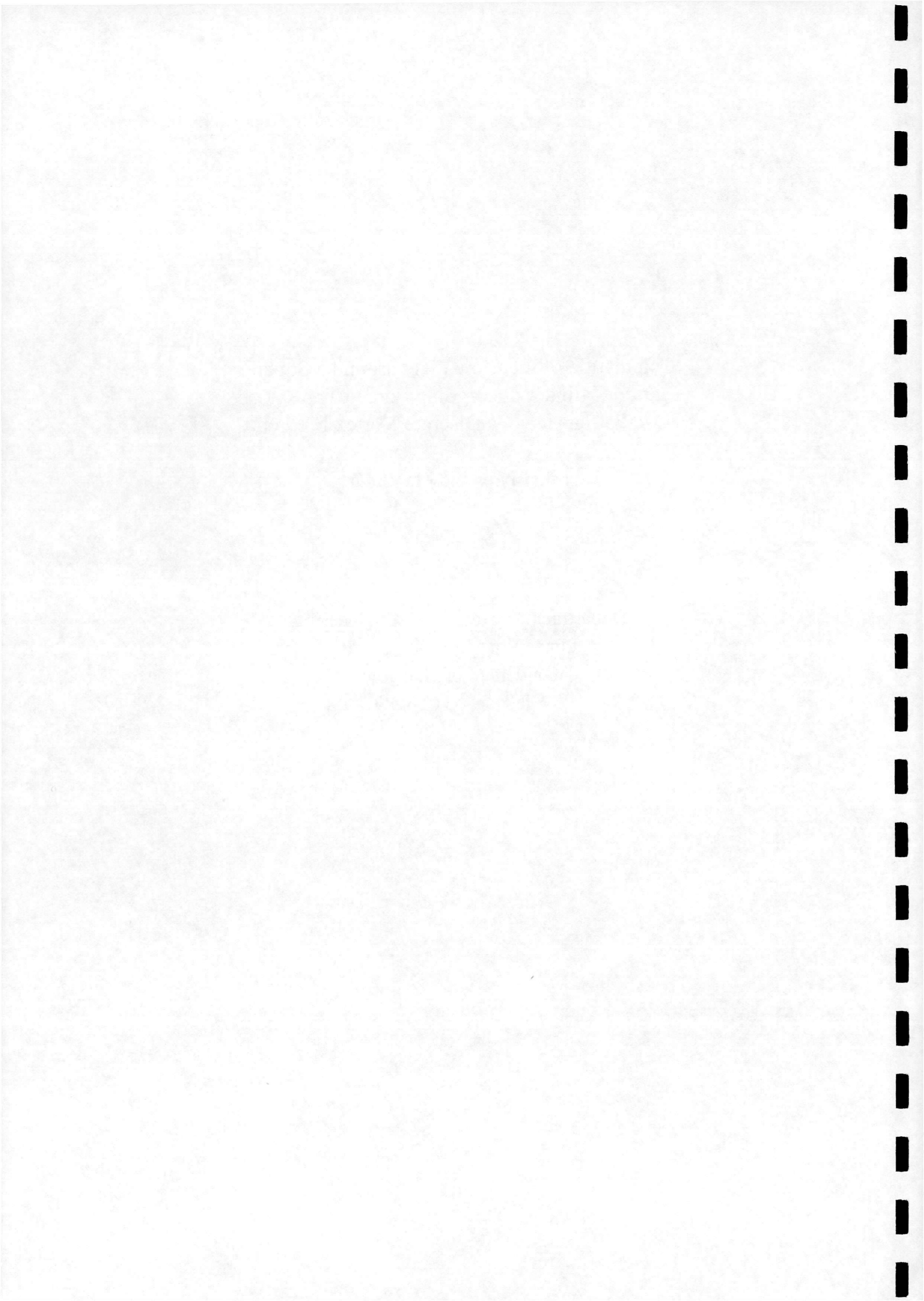
I. J. Taylor and M. Vezza



Calculation of the Flow Field around a Square
Section Cylinder undergoing Forced Transverse
Oscillations using a Discrete Vortex Method.

I. J. Taylor and M. Vezza

Department of Aerospace Engineering
James Watt Building South
University of Glasgow
Glasgow G12 8QQ



Calculation of the Flow Field around a Square Section Cylinder undergoing Forced Transverse Oscillations using a Discrete Vortex Method.

Ian Taylor¹ and Marco Vezza²

*Department of Aerospace Engineering, University of Glasgow, Glasgow, G12 8QQ, Scotland,
UK.*

ABSTRACT :

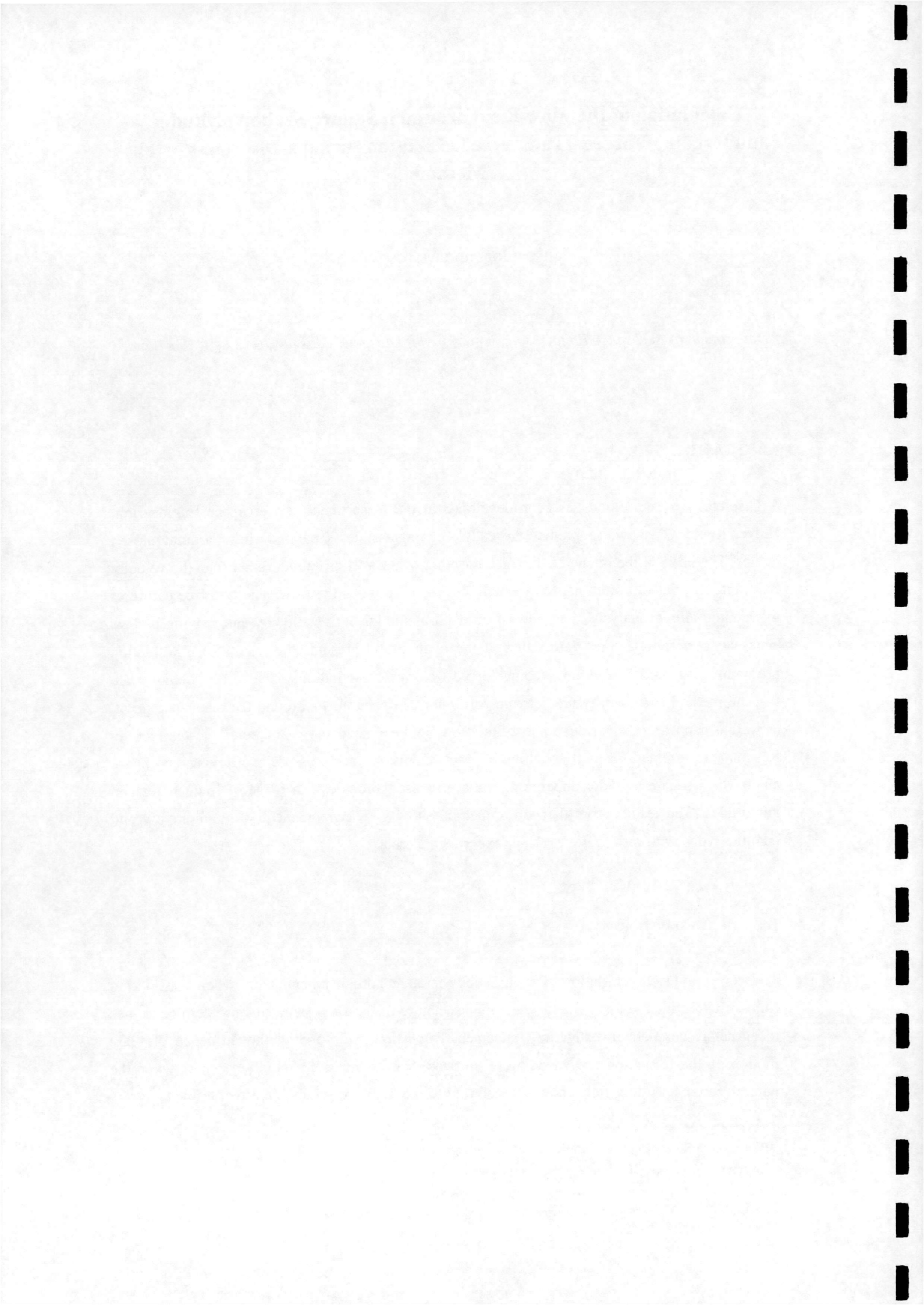
A Discrete Vortex Method has been developed at the Department of Aerospace Engineering, University of Glasgow, to predict unsteady, incompressible, separated flows around closed bodies. The basis of the method is the discretisation of the vorticity field, rather than the velocity field, into a series of vortex particles which are free to move in the flow. The grid free nature of the method allows analysis of a wide range of problems for both stationary and moving bodies. This paper presents a brief description of the method and presents the results of a validation programme on bluff bodies undergoing forced transverse oscillations. The results demonstrate that the method successfully predicts the vortex lock-in phenomena around the resonance point, as well as capturing the various states of the flow field expected above and below vortex lock-in. Results are presented for the fluctuating lift coefficients, surface pressure coefficients and phase angle, for a square cylinder undergoing transverse oscillations over a range of frequencies and amplitudes. The results from the vortex method show good agreement, both qualitatively and quantitatively, with results from various experimental data.

1.0 Introduction.

The vortex induced oscillation of a bluff body is an important phenomenon when considering fluid-structure interactions. Due to the complex nature of the flow field, this problem continues to attract researchers investigating fundamental questions surrounding the influence of body motion on the formation and shedding of vortices. Vortex induced oscillation occurs when the natural vortex shedding frequency is transferred to the body frequency, an effect termed "vortex

¹ Postgraduate Researcher : Department of Aerospace Engineering.

² Lecturer : Department of Aerospace Engineering.

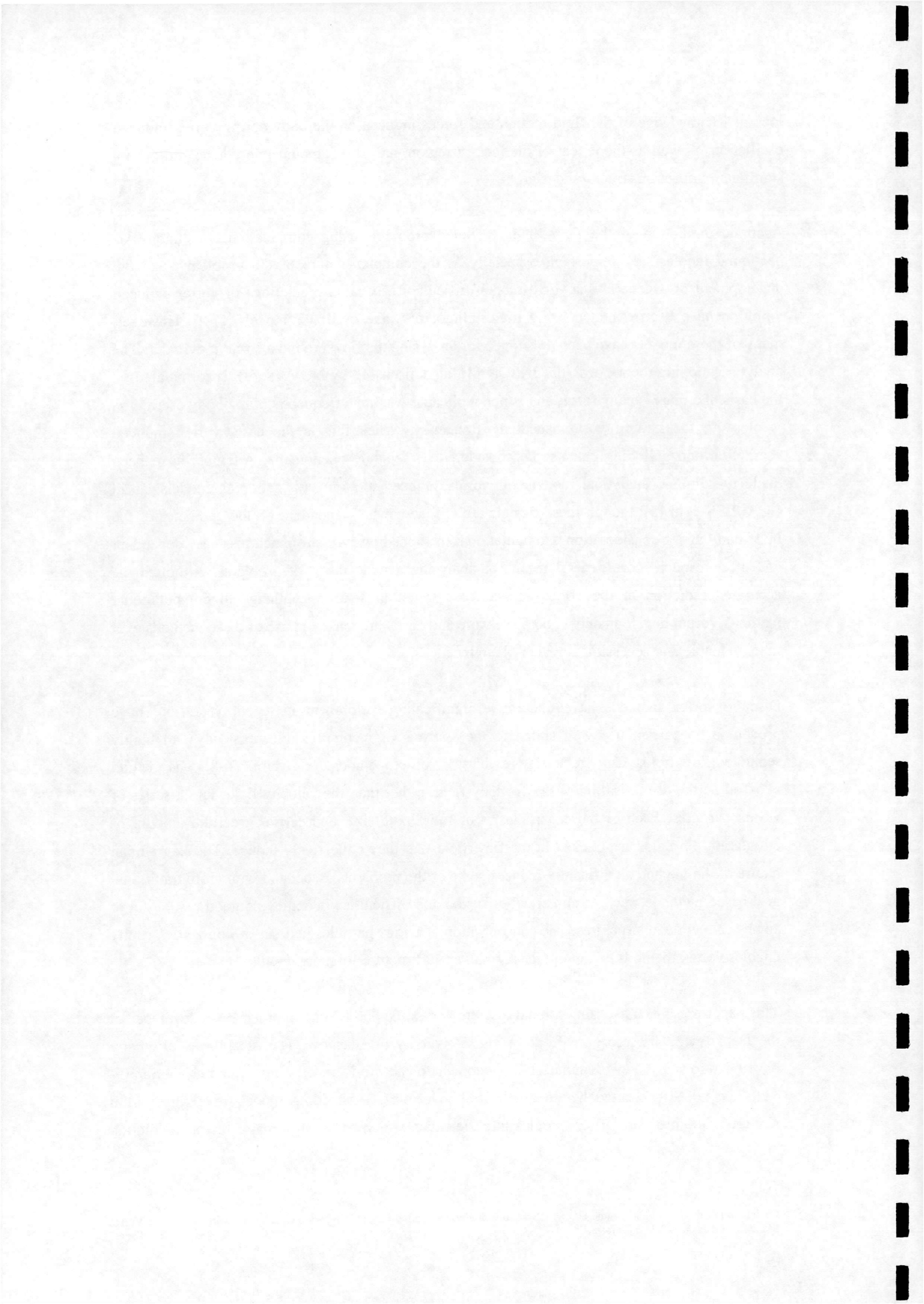


lock-in". Knowledge of the fluid motion and forces induced on the body during vortex induced oscillation, as well as the extent of the lock-in region, are of paramount importance and have a significant impact on structural design.

Accurate prediction of the flow fields for such problems using computational techniques is becoming increasingly important, especially as the complex nature of the problem make the development of a general analytical model difficult. Reasonable predictions of vortex induced vibration have been obtained using lift oscillator or wake oscillator models. [1-2]. However, many of these models have been developed for analysing the flow around a circular cylinder. The analytic galloping theory of PARKINSON [3], also discussed by NOVAK [4], is formulated on the basis of a quasi-steady force, and is not applicable when the frequency of the body oscillation is close to the natural vortex shedding frequency. When this is the case, vortex induced oscillation and galloping can not be considered as separate phenomena. Attempts have been made to combine analytical models for vortex induced motion with galloping models, as in CORLESS et al [5], though these models are still somewhat dependent on the geometry of the bluff body under consideration. Computational methods however, are much less case dependent and offer a much more general means of analysing a wide range of problems. Although the accurate prediction of the vortex induced oscillation presents a challenge to computational methods, recent developments in both software and hardware make the use of these methods ever more valuable and accessible to the civil engineer.

Discrete vortex methods have undergone significant development in recent years and have proven to be particularly well suited to the analysis of incompressible, unsteady and highly separated flow fields. Comprehensive reviews of vortex methods are given in [6-8]. The method is based on the discretisation of the vorticity field, rather than the velocity field, into a series of vortex particles. Each of these particles is of finite core size, and carries a certain amount of circulation. Particles are tracked in the flow field that they collectively induce. The Lagrangian nature of the method significantly reduces some of the problems associated with more traditional grid based methods, such as numerical diffusion and difficulties in achieving good resolution of small scale vortical structures. The concentration of vortex particles in areas of non-zero vorticity enables vortex methods to capture these small scale structures in more detail.

This paper presents a two dimensional discrete vortex method (DVM) that has been developed at the Department of Aerospace Engineering, University of Glasgow. The model was originally developed to analyse the dynamic stall phenomena on aerofoils undergoing a pitching motion [9-11]. The DVM presented herein employs a novel surface shedding model, involving partial release of the nascent vortex particles into the wake, which has been a major factor in solution



quality to date. The grid free nature of the method makes it well suited to the analysis of bodies undergoing oscillatory motion.

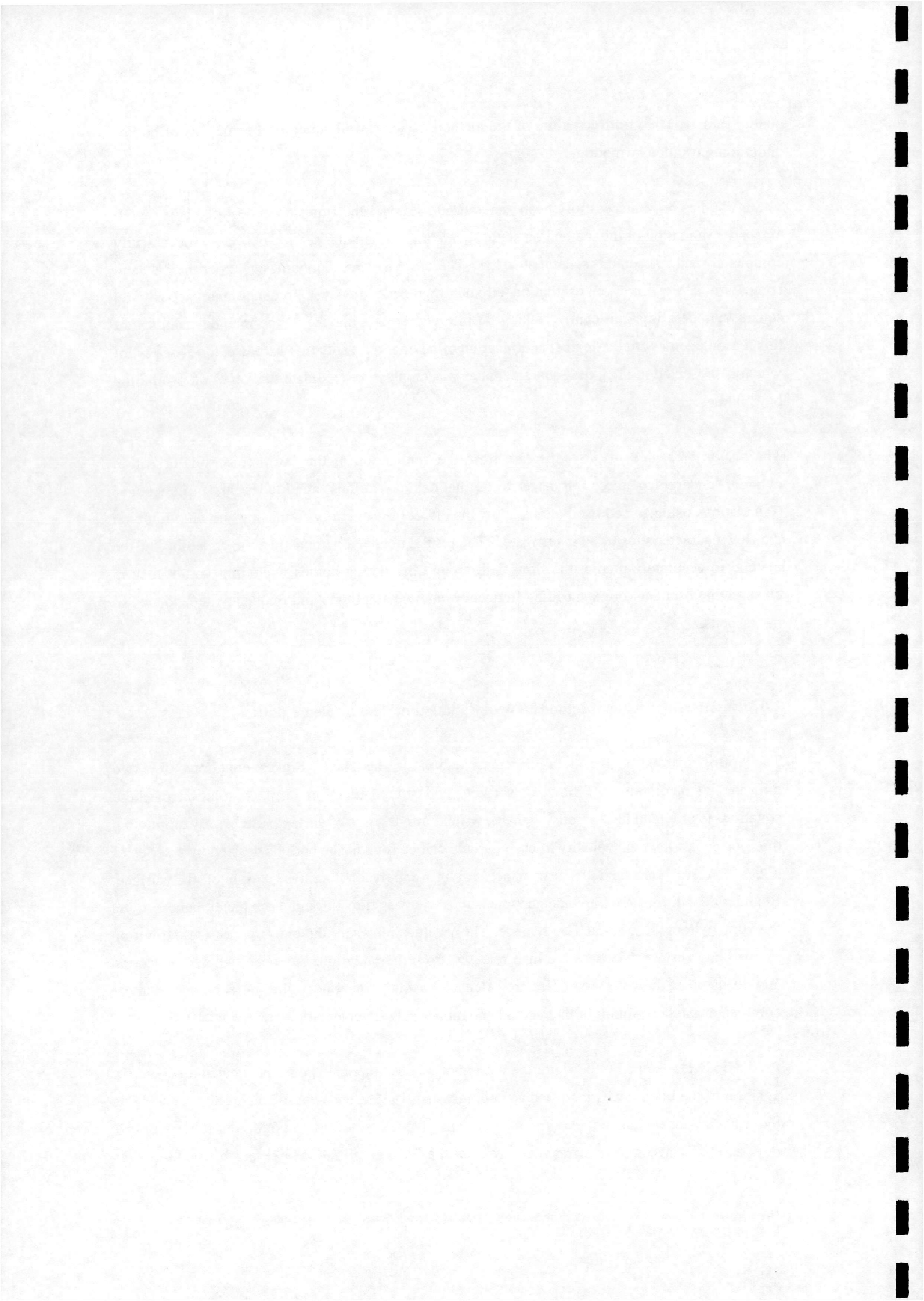
The DVM has now successfully been generalised to model the flows around bluff bodies, with extensive validation of the method on static square and rectangular section cylinders successfully completed and presented separately [12]. There is a large amount of experimental and computational research on oscillating circular cylinders, however computational activity on square cylinders is significantly lacking despite numerous published experimental results. For this reason, along with the logical continuation of an ongoing validation exercise, the first part of which is presented in [12], the square cylinder was employed to validate the DVM on oscillating bluff bodies.

The results presented in this paper are from the application of the DVM to a square section cylinder undergoing forced transverse oscillations at various amplitudes and frequencies. Calculations using forced oscillations allow the effect of oscillatory frequency and amplitude on the flow characteristics to be investigated. The results obtained demonstrate the capability of the method to accurately predict the flow field around oscillating bodies, including vortex lock-in close to the resonant vortex shedding frequency, and the amplitude and frequency dependency of the response.

2.0 Discrete Vortex Method : Theory and Numerical Implementation.

The vortex method is based on a representation of the Navier-Stokes equations, for two dimensional incompressible flow, in vorticity and stream function form. A solution of these equations is provided by discretising the flow field into a series of vortex particles. By employing the Biot-Savart law, the velocity of each particle can be found. The body is defined by a series of nodes that are connected to form panels, giving a polygonal representation of the surface. Boundary conditions are implemented to ensure zero mass flow through each panel, hence giving the vortex strength, γ , at each body node. The γ values represent the entire vorticity distribution on the body surface. Vortices are then released from the body into the wake, where convection and diffusion of the vortex particles are calculated using an operator splitting technique. A more comprehensive description of the method and numerical implementation are given in [9-11].

As the body is assumed to be rigid, the motion of a body reference point, c , is calculated and the position of the body nodes modified accordingly using a reference coordinate system (Fig. 1). In the calculations presented herein, the body is given a sinusoidal motion in the transverse direction (normal to the freestream velocity) with a fixed amplitude. However, the model is such



that any single or combined motion, either transverse, longitudinal or rotational, can easily be applied. The acceleration that accompanies the body motion produces extra forces acting on the vortex particles resulting in additional surface pressure gradients. These are accounted for in the calculation of the pressure distribution on the body surface [9-11].

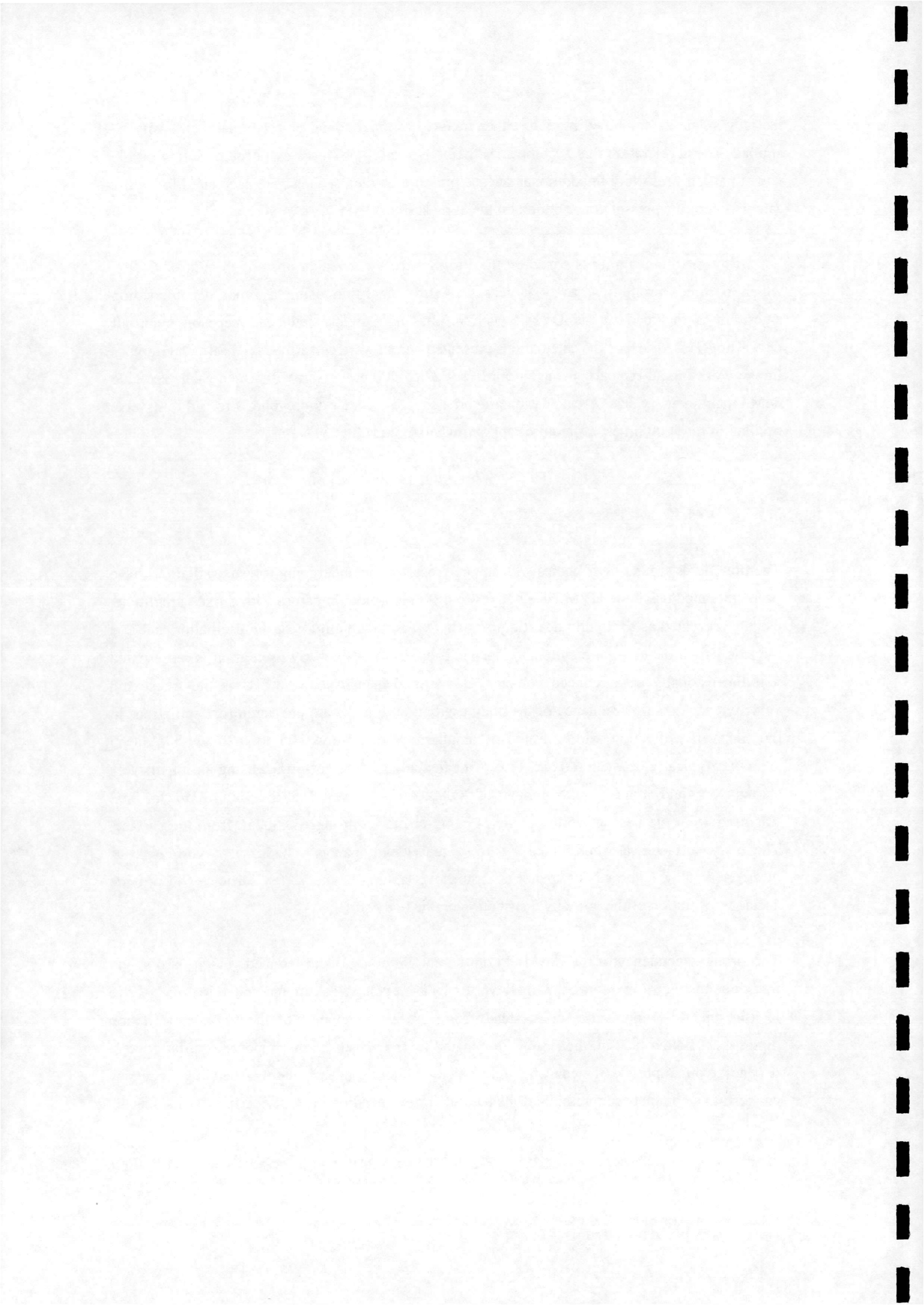
For a flow field containing N particles, the Biot-Savart law gives an operation count of $O(N^2)$, which becomes prohibitive as N increases. A fast algorithm using a zonal decomposition algorithm is included in the DVM which results in a greatly reduced operation count of $O(N+N\log N)$ [13]. All of the calculations presented herein were performed on a Silicon Graphics Indigo workstation, typically using a 150MHz IP22 R4400 processor, with 16Kb cache size and 64Mb main memory size. A calculation around a square cylinder undergoing a forced transverse oscillation for 9000 timesteps requires approximately 33hrs CPU.³

3.0 Results and Discussion.

The flow fields around bluff bodies with square cross section undergoing forced oscillations have been computed using the DVM. The body forcing is sinusoidal in nature with a fixed amplitude, usually presented as an amplitude ratio, a/L , where a is the amplitude of the oscillation and L is the side length of the square cylinder (Fig. 1). The period of the body oscillation is represented non-dimensionally as a reduced velocity, U_r , defined as $U/N_b L$, where U is the freestream velocity and N_b is the frequency of the body oscillation. Results are presented for oscillations in the transverse direction with a range of amplitude ratios from 0.05 to 0.25, with reduced velocities typically between 4.0 and 11.0. All calculations were performed using an impulsively started flow field, at a Reynolds number of 20000. A non-dimensional timestep, $\Delta t U/L$, of 0.02 was used, with the nascent vortex particles being created a distance $0.0025L$ from the surface. The body surface was represented by 160 equal length panels. The nascent vorticity was discretised using 7 vortices per panel to ensure overlapping of the vortex particles and provide accurate resolution of the vorticity distribution on the body surface.

The strong dependency of the flow field on the amplitude ratio and reduced velocity a division into three distinct flow regimes, namely vortex lock-in, below lock-in and above lock-in. Above lock-in, the flow approaches quasi steady form as the dominance of the forcing oscillation diminishes. Below lock-in, the flow is dominated by the effects of the imposed oscillation and, depending on amplitude, the concentrated vorticity which is generated at the shedding frequency can lead to a complete suppression of the natural vortex shedding mode. Lock-in is defined as the

³Stationary square at 0° incidence used 25hrs CPU for 7000 steps (12.9secs/step compared with 13.2secs/step in oscillating case). Note that the CPU is not significantly increased in the calculation with body motion.

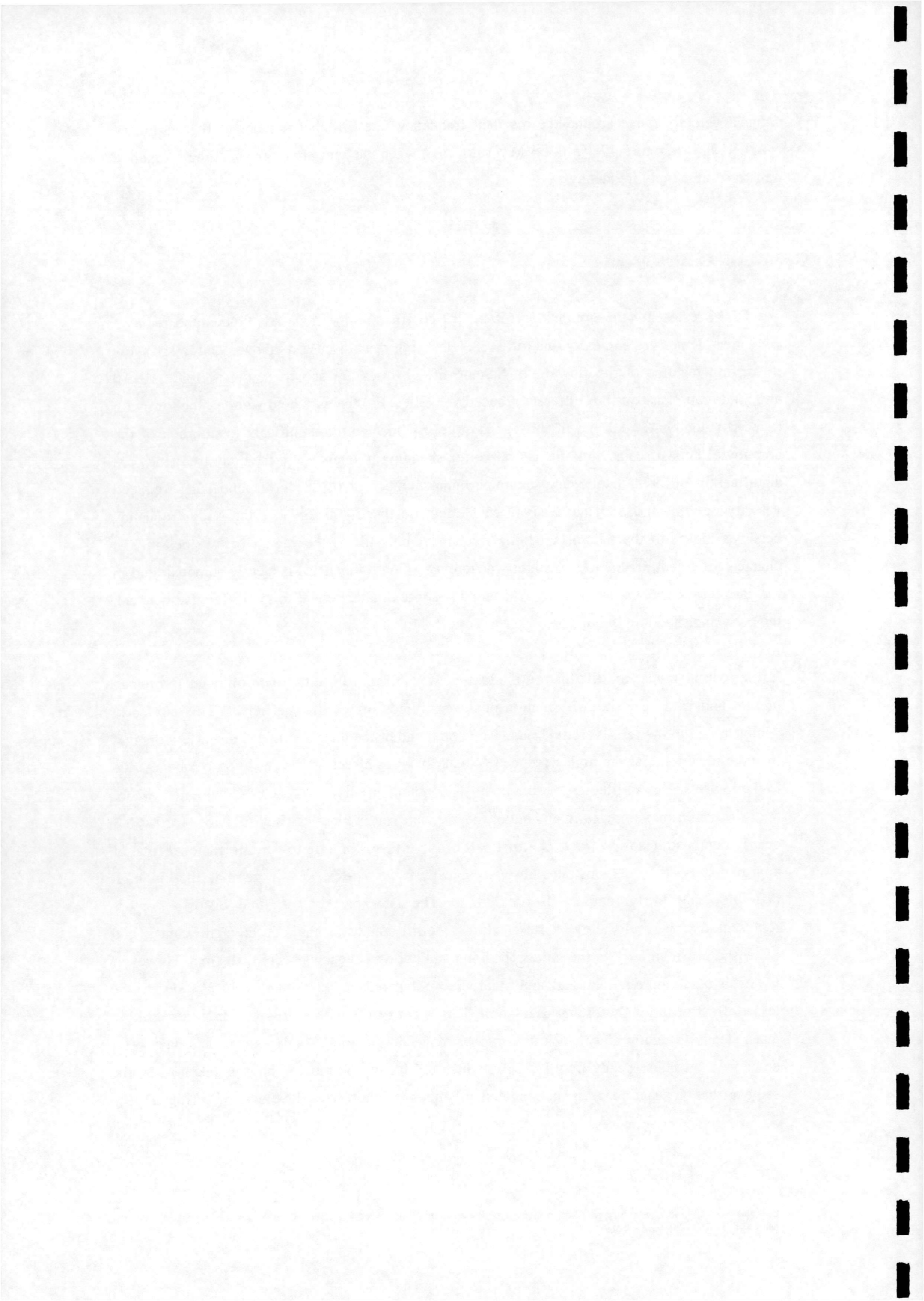


reduced velocity range around the resonant frequency (the Strouhal number of the stationary cylinder, shown to be 0.128 from DVM results [12]) when the natural vortex shedding frequency transfers to the body frequency.

3.1 Analysis of Lift History.

The DVM results for the time history of the lift coefficient at various amplitudes and reduced velocities demonstrate clearly the different flow regimes discussed above, and also show interesting features of the flow field. Sample lift histories are shown in Fig. 3 for the 0.10 amplitude ratio case, at four different reduced velocities. For the case below vortex lock-in, with reduced velocity, $U_r=5.0$, the lift history is quite irregular with a significant modulation of the amplitude. This arises as both the natural vortex shedding frequency and the body frequency are significantly different (stationary square Strouhal number of 0.128 corresponds to a reduced velocity of 7.8), and each has a significant effect on the lift history. As the body frequency becomes closer to the natural shedding frequency, but still in the region below lock-in, the characteristic beating due to two slightly different forcing frequencies is clearly demonstrated in the case with $U_r=6.75$. The beating frequency is approximately equal to the difference between the body and shedding frequencies.

In the lock-in range, the lift history is close to sinusoidal, with only one dominant frequency present and with very little modulation of the amplitude of the lift coefficient. This is clearly demonstrated in the results from $U_r=8.0$. The upper end of the lock-in range is much less distinct than the lower end, as the higher reduced velocity has less effect on the shedding frequency due to the lower energy oscillations of the body. This results in a range of reduced velocities where the flow condition is moving in and out of the resonant vortex lock-in. The lift history for $U_r=8.3$ clearly demonstrates this effect. The first part of the time history, up to non-dimensional time of approximately 120, demonstrates results typical of the vortex lock-in region, that is high amplitude and fairly regular lift oscillations. The later part of the time history is more representative of results above vortex lock-in : the lift amplitude has reduced significantly, and increased in irregularity as the vortex shedding and body frequencies become distinct. However, the lift is much more regular and sinusoidal when compared to the case below lock-in due to the lesser effect of the body forcing oscillation. This is consistent with a flow which is increasingly quasi-steady in nature above lock-in at higher reduced velocities. Analytical models have been developed for quasi-steady flow [3, 4], in which the lift on the moving body is taken to be the same as that on a stationary cylinder at angle of attack α , in a flow with velocity U_{rel} (Fig. 2).



3.2 Vortex Shedding Frequency Measurements.

Spectral analysis was performed on the lift histories with the results being used to ascertain the reduced velocity range at which vortex lock-in occurs for each amplitude ratio. Away from lock-in, the vortex shedding frequency and the body frequency can be seen as two distinct peaks in the frequency analysis. At vortex lock-in, the shedding frequency is modulated to the body frequency, and a single peak is seen in the frequency analysis. Both of these phenomena are demonstrated in the results of the DVM calculations, samples of which are given in Fig. 4.

The vortex shedding frequency, n_s , is estimated from these power spectra, and is shown, divided by the body frequency, N_b , plotted against U_r in Fig. 5. The straight lines in the figures show the ratio between the Strouhal number of the stationary body and N_b . Outside of vortex lock-in, the ratio n_s/N_b should be approximately on this line. In the lock-in region, the ratio becomes equal to unity as the shedding frequency is transferred to the body frequency. This is clearly demonstrated in the results from the DVM. Compared with experimental data [14, 15], the region of vortex lock-in is well predicted for both the 0.1 and 0.15 amplitude ratios. The most noticeable feature of the results is the wider lock-in range as amplitude ratio increases. Again, this effect is well predicted by the DVM.

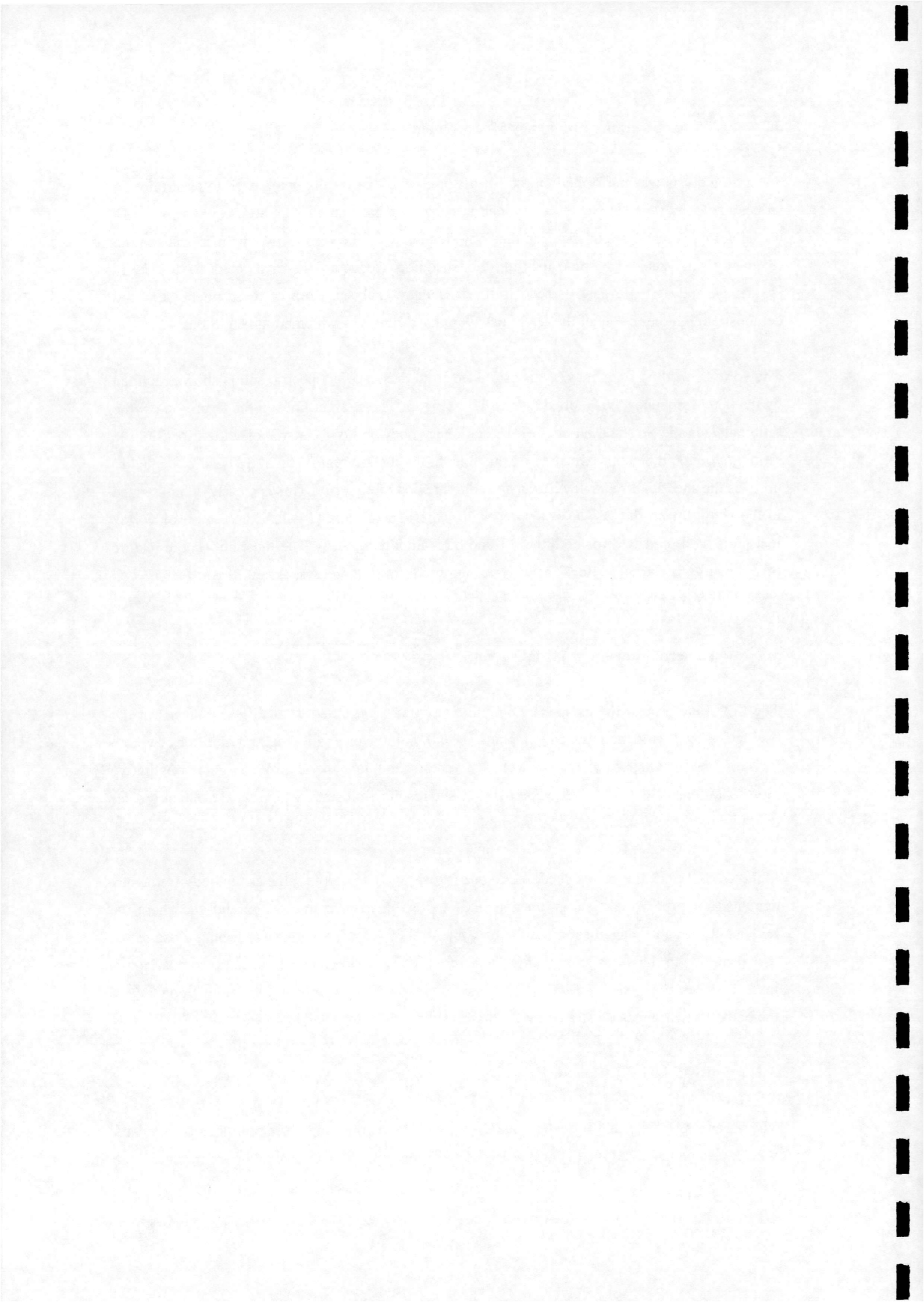
3.3 General Flow Field Visualisation.

The flow field around the oscillating body is presented (Fig. 6 and 7) at different stages of the oscillatory cycle, for the reduced velocities $U_r=6.0$, below vortex lock-in, and $U_r=8.0$, in vortex lock-in. The results are shown as velocity vectors and in general provide good qualitative representations of the flow field. Compared to the results on a static square [12] a much greater modulation of the wake is clearly discernible.

In the $U_r=8.0$ case, the vortex shedding frequency is quite clearly the same as the body frequency demonstrating the vortex lock-in phenomena. This is apparent from Figs. 7a and 7e, where the body is at the same stage of the oscillation cycle. In both cases, a vortex is forming close to the rear face, due to the shear layer that is shed from the lower side face. If the same comparison is made between Figs. 6a and 6e, it is clear that vortex shedding occurs at a different frequency to the body oscillation, as illustrated by the dissimilar stages of the shedding cycle.

3.4 RMS Lift Coefficient, C_{Lrms} .

The variation of the rms lift coefficient, C_{Lrms} , with U_r over a range of amplitudes is compared with experimental data [16, 17] in Fig. 8. The variation of C_{Lrms} can be explained by considering



the different flow regimes. At low U_r , below lock-in, concentrated vorticity is generated and shed at the body frequency, resulting in the natural vortex shedding mode being suppressed. This leads to a reduction in the fluctuating lift force on the body, an effect which is magnified with increasing oscillation amplitude. In the lock-in region, C_{Lrms} gradually increases until the maximum value is reached at the resonance point. Just above lock-in, the sharp decrease in the C_{Lrms} corresponds with the separation of the vortex shedding and body frequencies. An interaction occurs between the vortex formation and the rear corners on the square which reduces the strength of the vortex, producing the decrease in C_{Lrms} . As U_r is increased further, the flow approaches a quasi steady form, with C_{Lrms} gradually approaching the value found on the stationary body (equal to 1.37 in the DVM and 1.12 in LU, CHEN et al [16]⁴).

The results from the DVM demonstrate the variation discussed above and show generally good agreement with experimental data. It should be noted that some of the discrepancies can be attributed to the differences in the range of U_r for which lock-in is assumed. For example, the 0.25 amplitude ratio case has a lock-in range of approximately $U_r=5.5$ to 12.0 in the experiments [14, 17], whereas the DVM lock-in range is from 4.5 to 9.0. It can be shown that the lock-in is somewhat sensitive to Reynolds number, with a larger range of U_r expected at lower values. The Re employed in the DVM was chosen to be representative of all the experimental data being used for comparison but differs from each dataset to some degree. The results for the lowest amplitude ratio, 0.05, are more difficult to interpret as only a very small lock-in region was predicted at $U_r \approx 7.5$. Also, the vortex shedding is more dominant making the effects of body oscillation sometimes difficult to detect.

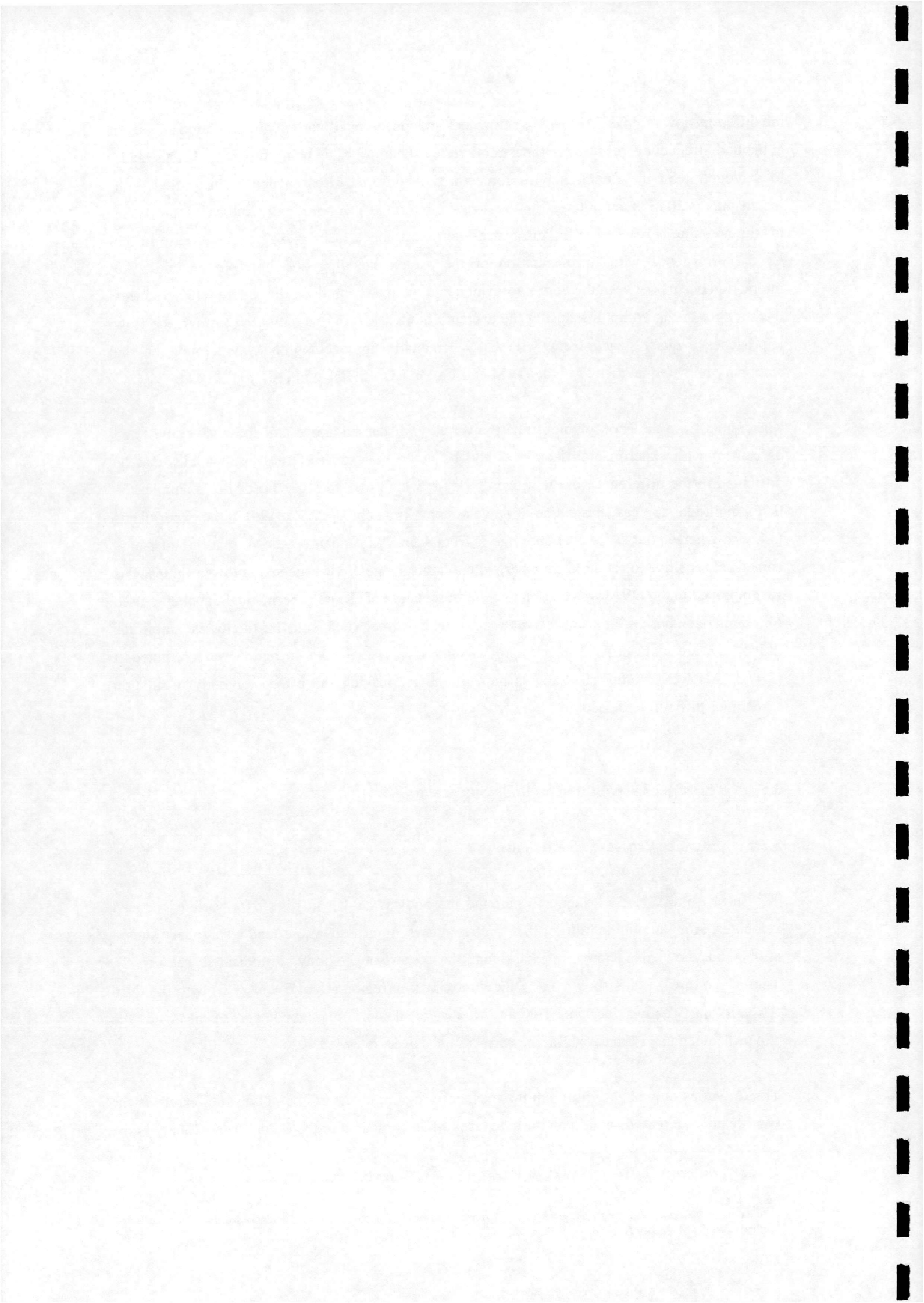
3.5 Pressure Distribution on Body Surface.

3.5.1 Surface Pressure Coefficient.

The surface pressure coefficient, C_p , around the body is shown in Fig. 9 for various reduced velocities, at an amplitude ratio of 0.25. For comparison purposes C_p around a stationary square at 0° incidence is also shown. In each figure, the corners of the body are indicated (see Fig. 2). Two of the three results shown are in the vortex lock-in region ($U_r=7.5$ and 7.75) with the third ($U_r=8.5$) just above lock-in. The DVM results demonstrate good agreement with the experimental data [14] and exhibit the correct trends as U_r is varied.

The C_p varies only slightly through the resonance region, however one noticeable feature is the significantly increased suction on the side faces when compared to the C_p on the stationary body.

⁴Various experimental data shows that C_{Lrms} is generally within the range 1.20 to 1.35 [12].



During lock-in, the vortices shed from the body are stronger due to the effect of the body oscillation, giving rise to the higher suction on the side faces. Above lock-in, the C_p on the side faces reverts to values closer to those seen on the static body, although there is a significant reduction in the base suction. LU and CHEN et al [16] found a similar effect with a reduction in the drag coefficient at reduced velocities just above lock-in. A conjectured reason for this effect is the significant interference of vortices forming from the side faces with the rear corners of the body at reduced velocities just above lock-in. This interference tends to move the vortex formation further downstream, reducing the base suction.

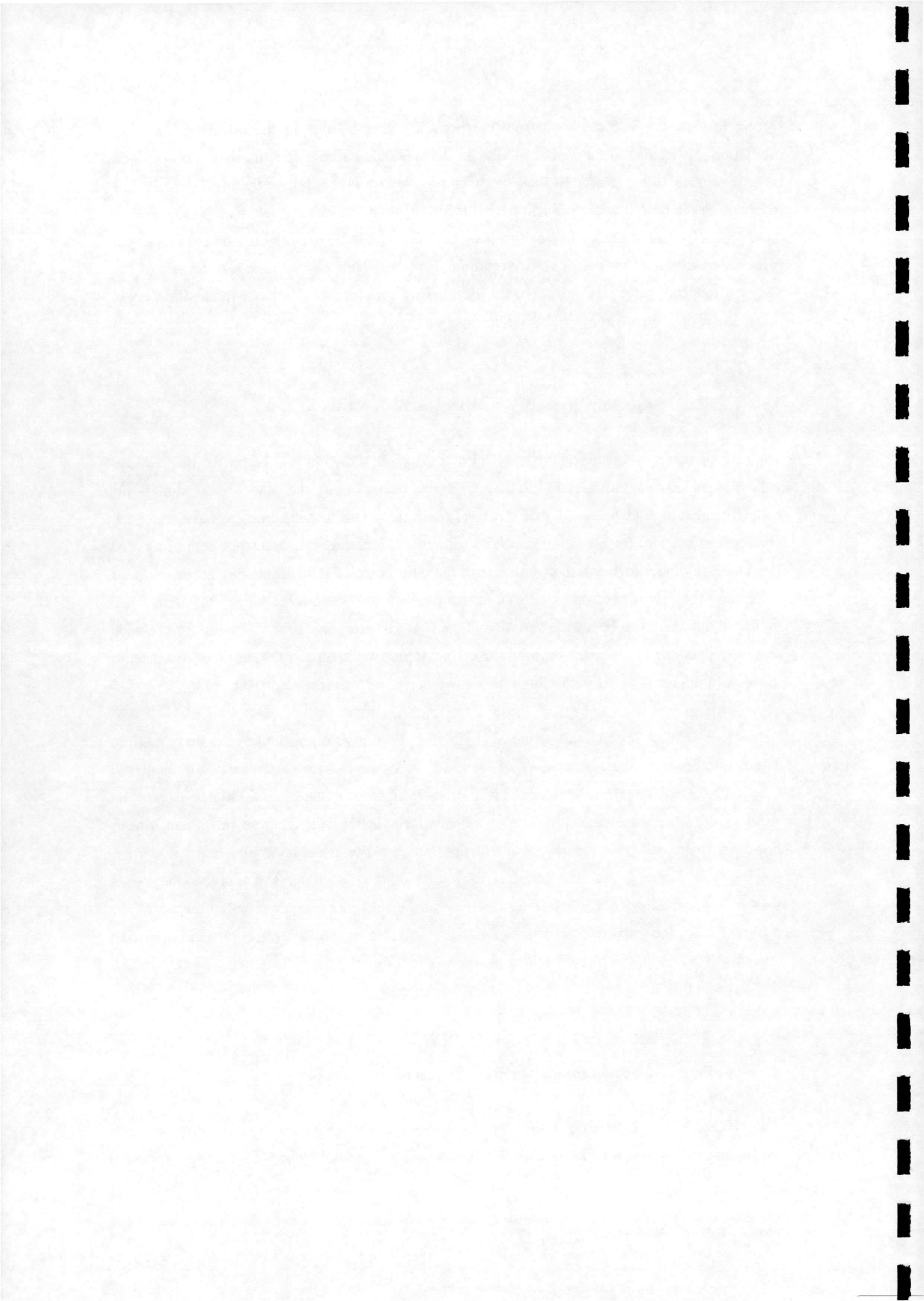
3.5.2 RMS Fluctuating Pressure Coefficient on Body Surface.

The rms fluctuating pressure on the body surface, C_{prms} , is shown in Fig. 10 for various reduced velocities at an amplitude ratio of 0.1, with the results from the static body shown for comparison. It should be noted that the measurements of fluctuating pressure have not been corrected to account for acceleration effects (due to the pressure transducer not being mounted flush to the cylinder surface), though the errors are only expected to be significant at low reduced velocities [14]. However, previous comparisons between various experimental data have indicated that there can be a wide variation in the C_{prms} results (Fig. 10a). Allowing for the wide scatter of data, the DVM results exhibit the correct trends with reduced velocity. For instance, in the lock-in region, C_{prms} is noticeably greater, with a maximum at the resonance point.

Below lock-in, C_{prms} is generally reduced slightly, as the flow is dominated by the body motion. The results towards the rear corners of the body do however show a tendency for increased C_{prms} . The relative angle of incidence of the freestream flow as the body oscillates, causes the shear layer to begin to reattach to one of the side faces of the body. Before full reattachment, however, there will be a significant interaction between the shear layer and the rear corner, leading to the higher C_{prms} in this region. Above lock-in, the C_{prms} begins to approach the results seen on the static model. The reduced velocities for the above lock-in case used in the DVM are different from the experimental values due to differences in the upper lock-in boundary (see section 3.1). The results of calculations just above lock-in are used ($Ur=8.5$ and $Ur=9.0$) which demonstrate the change in C_{prms} as the flow state changes.

3.6 Phase Angle and Frequency-Response Component of Lift.

The phase angle, ϕ , is defined as the angle by which the lift force leads the body displacement. From this definition, the lift is capable of sustaining free oscillations of a spring mounted



cylinder, when ϕ is within the range $0^\circ < \phi < 180^\circ$, the so called negative damping condition. The characteristic distribution for ϕ with varying U_r is demonstrated in the results from the DVM shown in Fig. 11. The most noticeable feature is the sudden increase from negative to positive phase angle through the lock-in region. It is clear that positive ϕ required for vortex induced oscillations only occurs once the reduced velocity is above the resonance point. This is also demonstrated in free oscillation experiments [15, 22]. The slope of the phase angle distribution also tends to decrease with increasing amplitude, giving further indication of the increased lock-in range at higher amplitude.

The results from the DVM demonstrate good agreement with experimental data (Fig. 12), although these data show a wide variation, highlighting the sensitive nature of the unsteady flow field. In addition, variations in the experimental flow conditions, such as Reynolds number, and variations in the static Strouhal number, may have had a strong effect on the results obtained from the oscillatory tests. However, the DVM results are within the range of experimental data, with the only discrepancy being the smaller predicted lock-in range at higher amplitudes discussed earlier. A favourable comparison can also be made with results obtained from a 3D CFD method [23] at amplitude ratios of 0.10 and 0.25.

The component of the lift history at the body frequency, or “frequency-response” component, may be expressed as

$$L_b(t) = L_0 \cos(2\pi N_b t + \phi) \quad (1)$$

where L_0 is the amplitude of the frequency-response component. This may be non-dimensionalised to give the frequency-response component of the lift coefficient

$$C_{Lb}(t) = C_{L0} \cos(2\pi N_b t + \phi) \quad (2a)$$

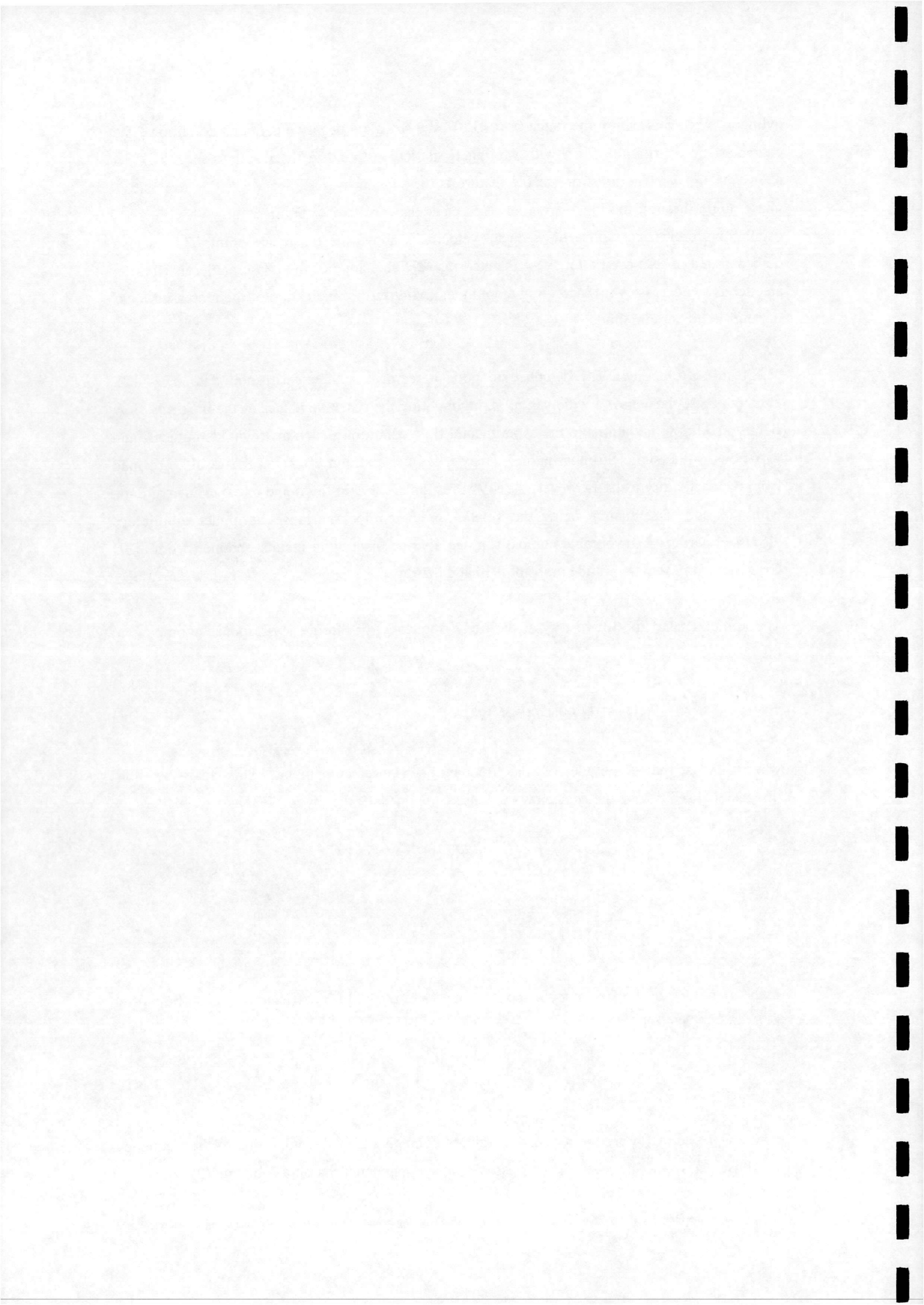
where

$$C_{L0} = \frac{L_0}{\frac{1}{2}\rho U^2 L} \quad (2b)$$

is the amplitude of the frequency response component of the lift coefficient. C_{Lb} can be written in complex notation

$$C_{Lb}(t) = \text{Re}[(C_{LbR} + iC_{LbI})e^{i2\pi N_b t}] \quad (2c)$$

where C_{LbR} and C_{LbI} are the real and imaginary components of the amplitude of the frequency-response part of the lift coefficient. These complex components can be obtained from (2)



$$\begin{aligned} C_{LbR} &= C_{L0} \cos \phi \\ C_{LbI} &= C_{L0} \sin \phi \end{aligned} \quad (3)$$

It may be noted that the condition for vortex induced oscillation is for C_{LbI} to be positive.

Comparisons of the frequency response amplitude, C_{L0} , with various experimental data are shown in Fig. 13. The most noticeable feature of the results is the approximate correspondence of the peak C_{L0} with the resonance point, and the increasing peak value with amplitude. The DVM results demonstrate good agreement with experiment, although the wide range of data should again be noted. Another feature to be noted is the C_{L0} values below lock-in tend to be higher than those above lock-in. This is indicative of the body oscillation having a more dominant effect on the lift force at the higher frequencies.

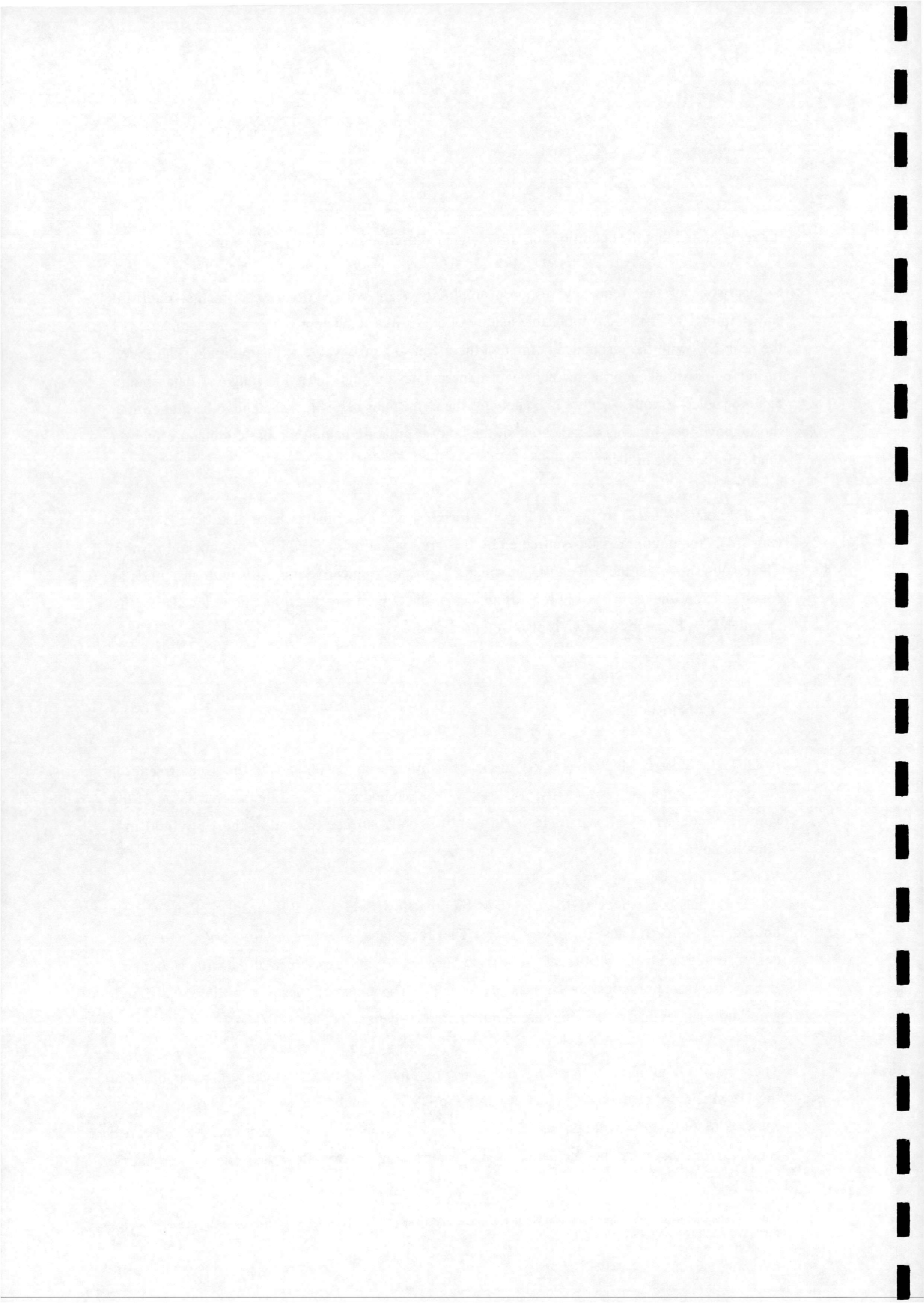
Good agreement between the DVM results for C_{LbI} and experiments have also been obtained (Fig. 14). Again, comparison is affected by the large variation in different experimental results. The results show that the value of U_r at which C_{LbI} becomes positive increases with amplitude as found in experiments. Allowing for differences in the experimental results, the reduced velocity at which C_{LbI} becomes positive is also well predicted.

4.0 Conclusions.

A Discrete Vortex Method (DVM) has successfully been developed at the Department of Aerospace Engineering, University of Glasgow. The method is based on the discretisation of the vorticity field, with vortex particles shed from the body surface tracked in the flow field in a Lagrangian manner.

The DVM has been successfully used to predict the flow field around a square section cylinder undergoing forced transverse oscillation. The resonance phenomena of vortex lock-in is demonstrated, with the results showing good agreement with experimental data for fluctuating lift and surface pressures, as well as phase angle. The trend of these quantities at different amplitudes and reduced velocities are demonstrated in the results of the DVM.

These results continue a successful validation programme and further enhance the capability of the DVM. Future research is aimed at using the DVM to analyse a wider range of geometries relevant to the field of wind engineering, such as suspension bridge deck sections. Also intended for future research is the inclusion of an dynamic solver, to allow analysis of aeroelastic



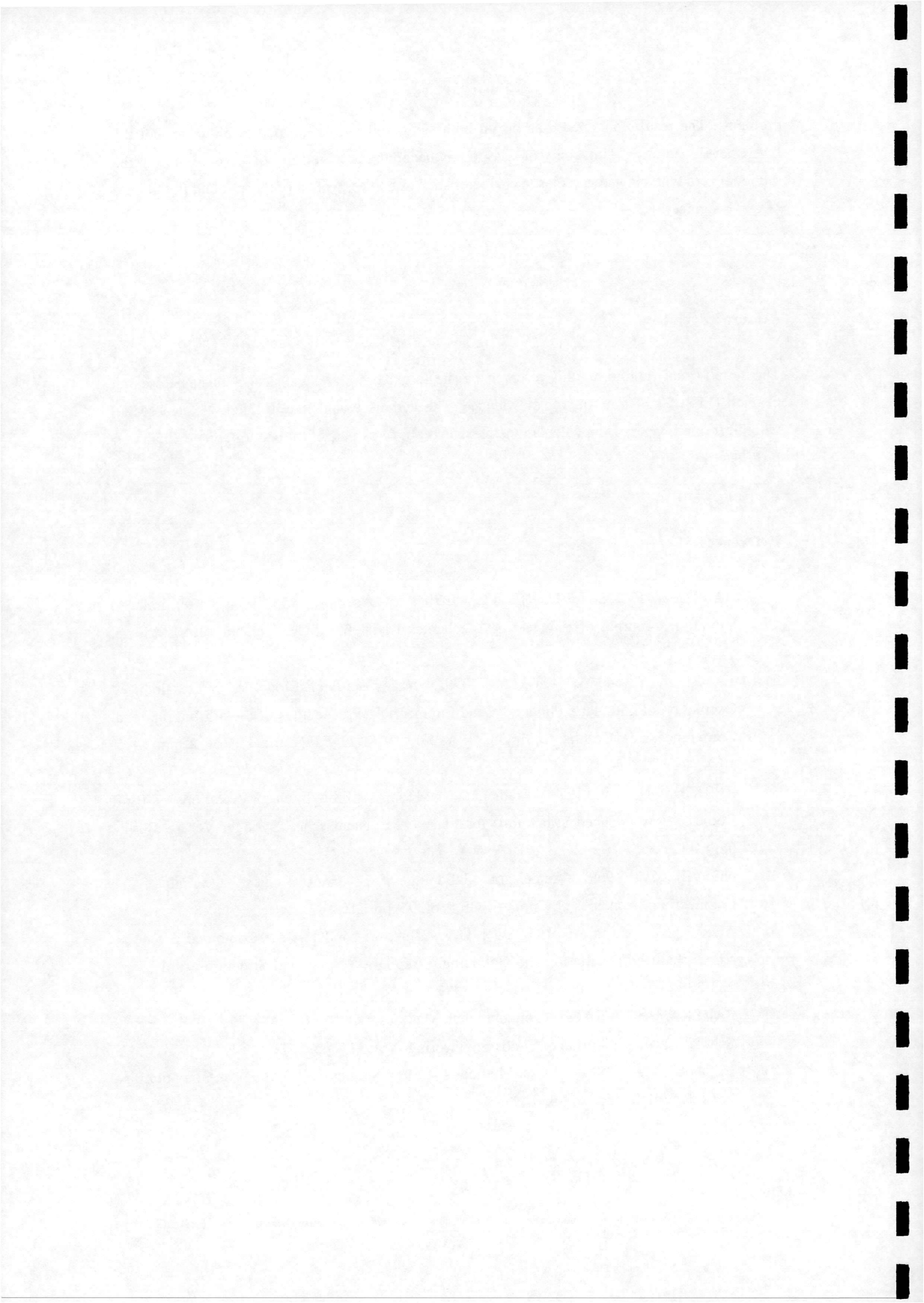
problems. The results obtained thus far on both static and oscillating bodies, indicate that the DVM developed at the University of Glasgow is becoming a powerful tool for determining the sectional aerodynamic and aeroelastic characteristics of bodies, typical of those found in the field of wind engineering.

Acknowledgements.

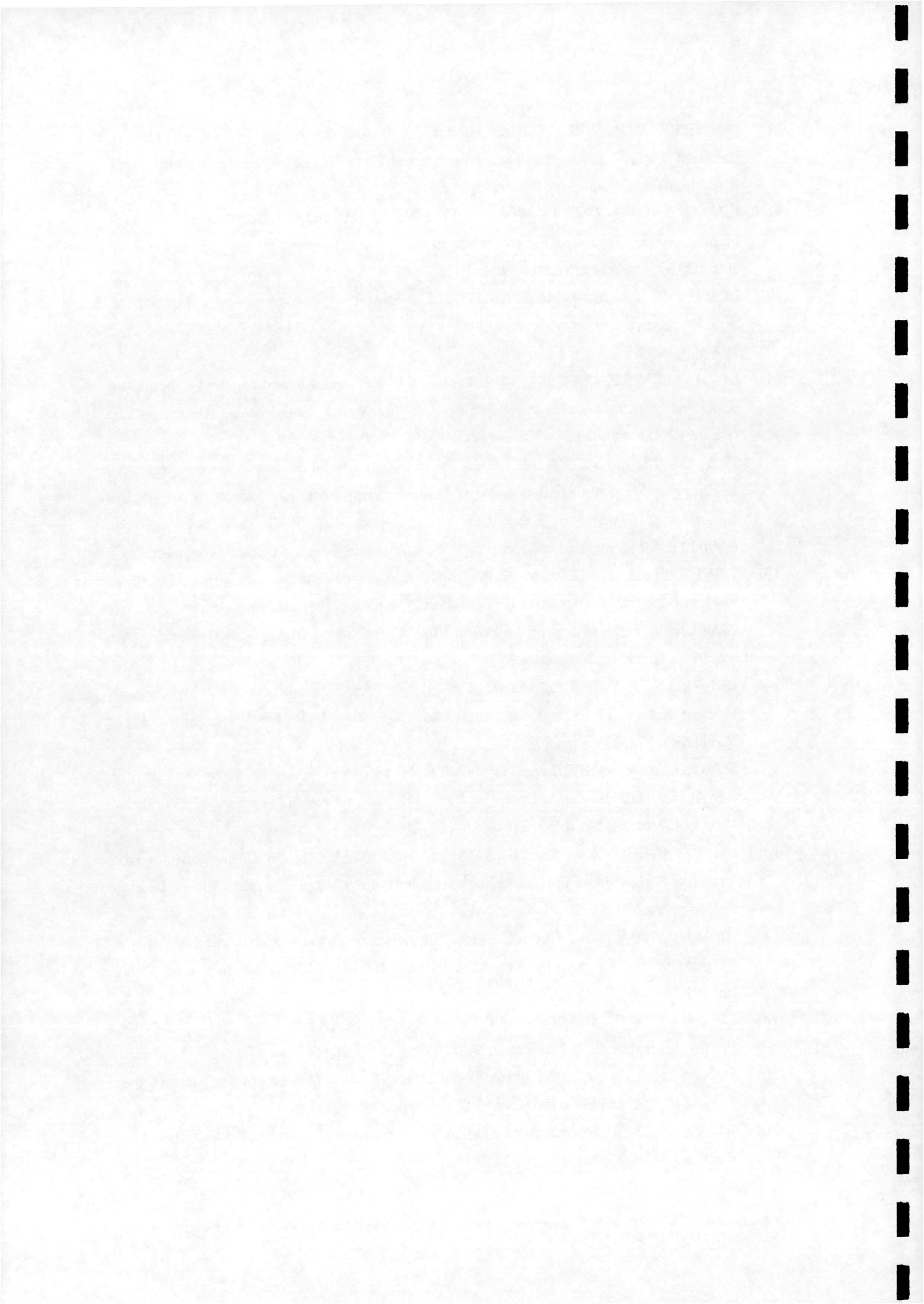
The support and funding of this research by the Engineering and Physical Sciences Research Council (EPSRC) is gratefully acknowledged. The authors would like to thank Mr. Rob Main who performed some of the calculations presented above as part of an undergraduate final year project.

References.

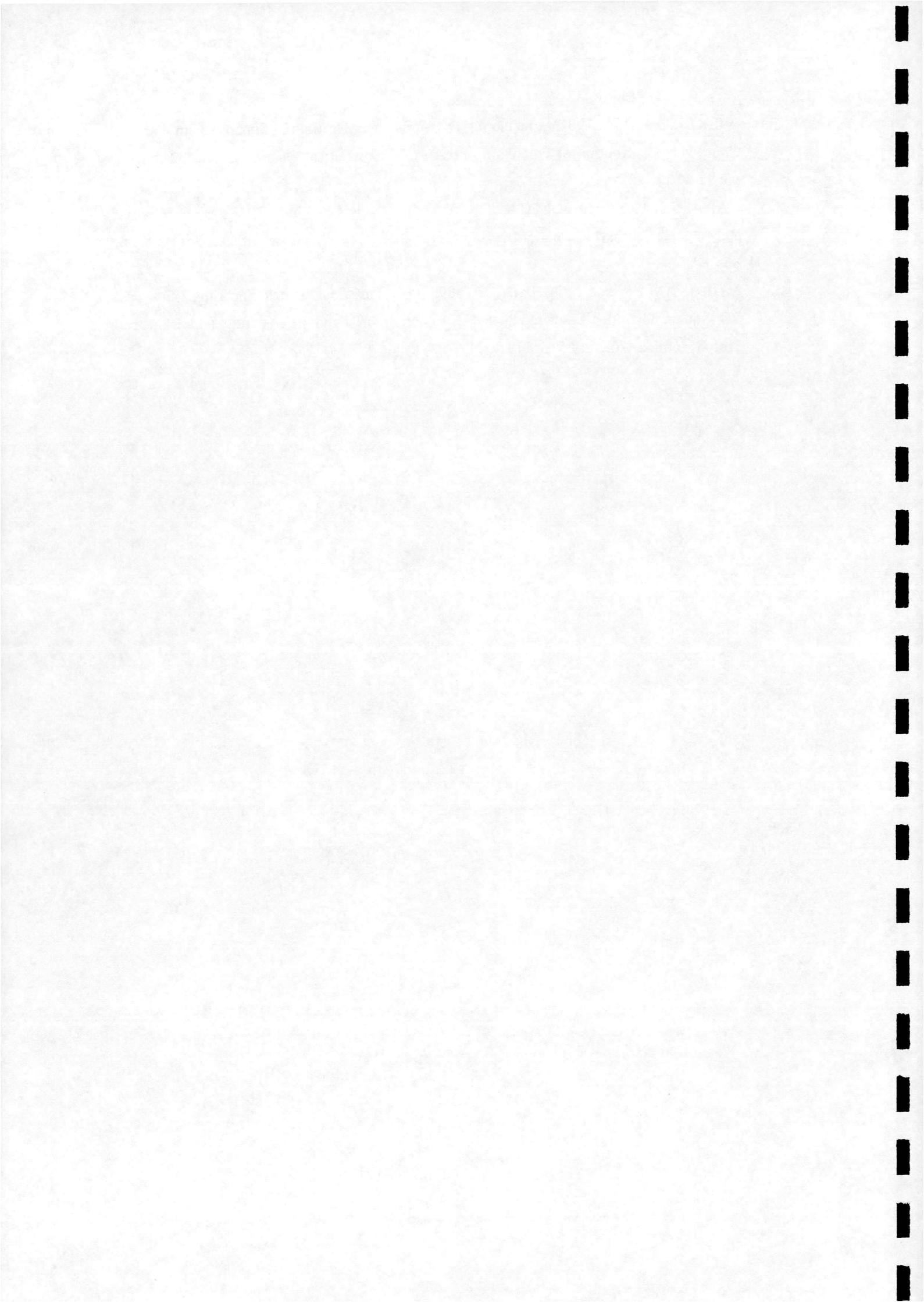
- 1) HARTLEN, R.T. and CURRIE, I.G., 1970, "Lift-Oscillator Model of Vortex-Induced Vibration." *Journal of Engineering Mechanics Division, ASCE*, Vol. 96, No. EM5, pp. 577-591.
- 2) TAMURA, Y. and MATSUI, G., 1979, "Wake-Oscillator Model of Vortex-Induced Oscillation of Circular Cylinder." *Wind Engineering, Proceedings of the 5th International Conference, Fort Collins, Colorado, USA, July 1979*, ed. J.E. Cermak, Vol. 2, pp. 1085-1094.
- 3) PARKINSON, G.V., 1974, "Mathematical Models of Flow-Induced Vibrations of Bluff Bodies." *Flow-Induced Structural Vibrations*, ed. E. Naudascher, Springer Verlag, Berlin, pp. 81-127.
- 4) NOVAK, M., 1969, "Aeroelastic Galloping of Prismatic Bodies." *Journal of the Engineering Mechanics Division, ASCE*, Vol. 95, pp. 115-142.
- 5) CORLESS, R.M. and PARKINSON, G.V., 1988, "A Model of the Combined Effects of Vortex-Induced Oscillation and Galloping." *Journal of Fluids and Structures*, Vol. 2, pp. 203-220.
- 6) SARPKEYA, T., 1989, "Computational Methods with Vortices - The 1988 Freeman Scholar Lecture." *Journal of Fluids Engineering*, Vol. 111, pp. 5-52.
- 7) LEONARD, A., 1980, "Vortex Methods for Flow Simulation." *Journal of Computational Physics*, Vol. 37, pp. 289-335.



- 8) PUCKETT, E.G., 1993, "Vortex Methods : An Introduction and Survey of Selected Research Topics." *Incompressible Computational Fluid Dynamics*, ed. M.D. Gunzb and R.A. Nicolaides, Cambridge University Press.
- 9) LIN, H. and VEZZA, M., 1996, "A Pure Vortex Method for Simulating Unsteady, Incompressible, Separated Flows around Static and Pitching Aerofoils." *Proceedings of 20th ICAS Conference, Sorrento, Italy*.
- 10) LIN, H., VEZZA, M. and GALBRAITH, R.A.McD., 1997, "Discrete Vortex Method for Simulating Unsteady Flow Around Pitching Aerofoils." *AIAA Journal*, Vol. 35, No. 3, pp. 494-499.
- 11) LIN, H and VEZZA M, 1994 "Implementation of a Vortex Method for the Prediction of Separated Incompressible Flows." Dept. of Aerospace Engineering, University of Glasgow, G.U. Aero Report No. 9425, Glasgow, Scotland, UK.
- 12) TAYLOR, I.J. and VEZZA, M., 1998, "Prediction of Unsteady Flow Around Square and Rectangular Section Cylinders using a Discrete Vortex Method." Dept. of Aerospace Engineering, University of Glasgow, G.U. Aero Report No. 9801, Glasgow, Scotland, UK. (submitted for publication in *Journal of Wind Engineering and Industrial Aerodynamics*.)
- 13) TAYLOR, I.J. and VEZZA, M., 1997, "Application of a Zonal Decomposition Algorithm, to Improve the Computational Operation Count of the Discrete Vortex Method Calculation." Dept. of Aerospace Engineering, University of Glasgow, G.U. Aero Report No. 9711, Glasgow, Scotland, UK.
- 14) BEARMAN, P.W. and OBASAJU, E.D., 1982, "An Experimental Study of Pressure Fluctuations on Fixed and Oscillating Square-Section Cylinders." *Journal of Fluid Mechanics*, Vol. 119, pp. 297-321.
- 15) OTSUKI, Y., WASHIZU, K., TOMIZAWA, H. and OHYA, A., 1974, "A Note on the Aeroelastic Instability of a Prismatic Bar with Square Section." *Journal of Sound and Vibration*, Vol. 34, No. 2, pp. 233-248.
- 16) LU, P.C., CHEN, R.H., CHENG, C.M. and HUANG, J.H., 1996, "Aerodynamics of a Vibrating Square Prism in Homogenous Turbulent Flows." *Journal of the Chinese Institute of Engineers*, Vol. 19, No. 3, pp. 353-361.
- 17) BEARMAN, P.W. and LUO, S.C., 1988, "Investigation of the Aerodynamic Instability of a Square-Section Cylinder by Forced Oscillation." *Journal of Fluids and Structures*, Vol. 2, pp. 161-176.
- 18) LEE, B.E., 1975, "The Effect of Turbulence on the Surface Pressure Field of a Square Prism." *Journal of Fluid Mechanics*, Vol. 69, Part 2, pp. 263-282.
- 19) HASAN, M.A.Z., 1989, "The Near Wake Structure of a Square Cylinder." *International Journal of Heat and Fluid Flow*, Vol. 10. No. 4, pp. 339-348.
- 20) IGARASHI, T., 1984, "Characteristics of the Flow Around a Square Prism." *Bulletin of the JSME*, Vol. 27, No. 231, pp. 1858-1865.



- 21) WILKINSON, R.H., 1981, "Fluctuating Pressures on an Oscillating Square Prism. Part 1 : Chordwise Distribution of Fluctuating Pressure." *Aeronautical Quarterly*, Vol. 32, No. 2, pp. 97-110.
- 22) NAKAMURA, Y. and MIZOTA, T., 1975, "Unsteady Lifts and Wakes of Oscillating Rectangular Prisms." *Journal of the Engineering Mechanics Division, ASCE*, Vol. 101, pp. 855-871.
- 23) MURAKAMI, S. and MOCHIDA, A., 1995, "On Turbulent Vortex Shedding Flow past 2D Square Cylinder Predicted by CFD." *Journal of Wind Engineering and Industrial Aerodynamics*, Vol. 54-55, pp. 191-211.



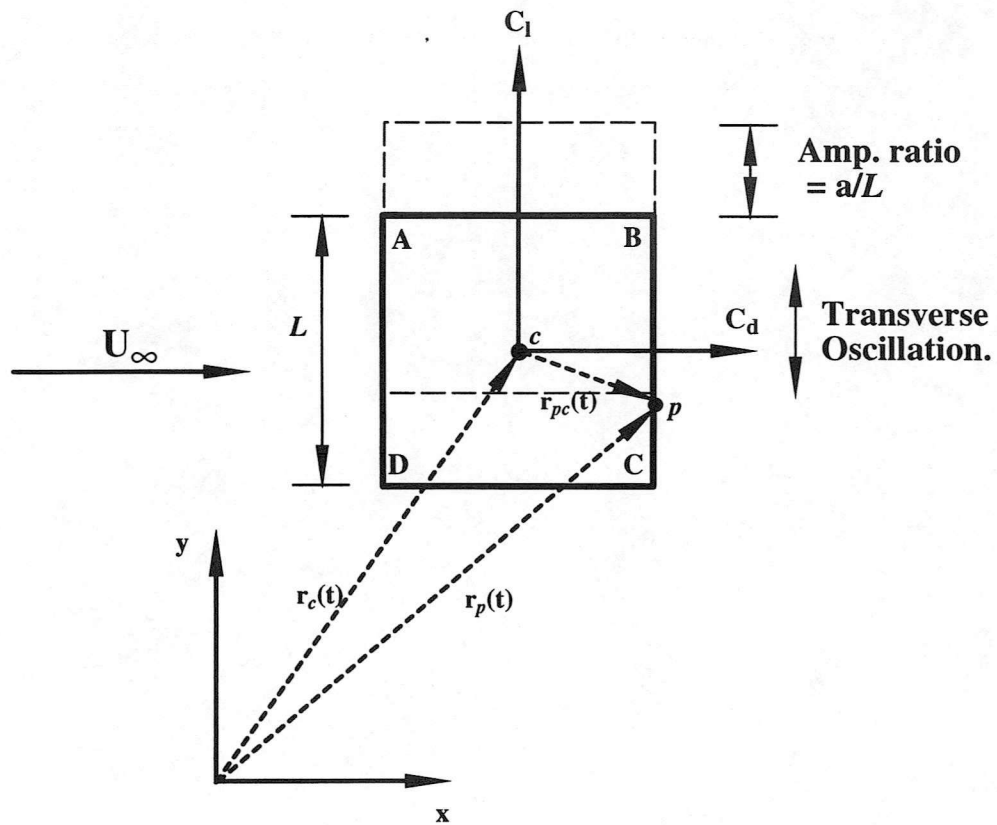


Fig. 1 - Body Orientation and Reference Coordinate System.

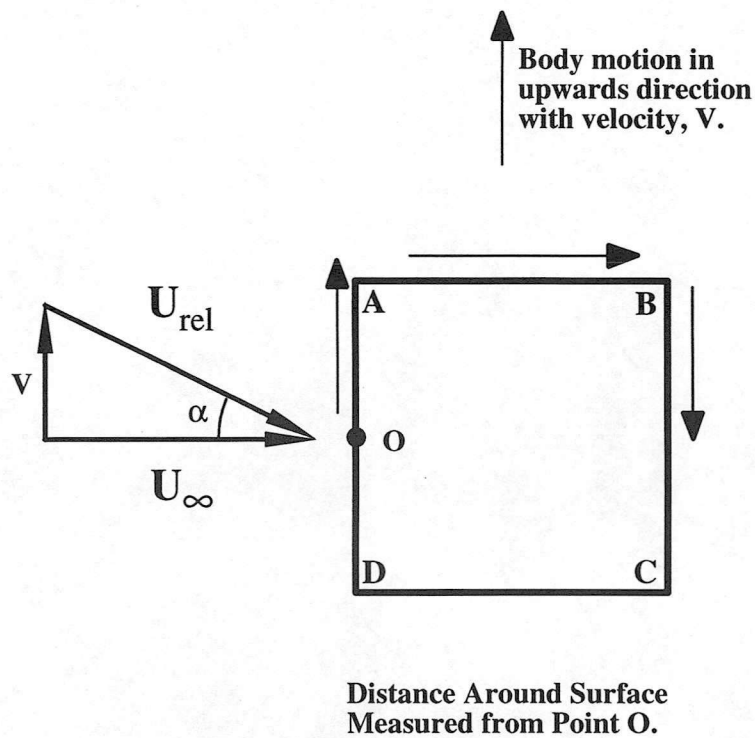
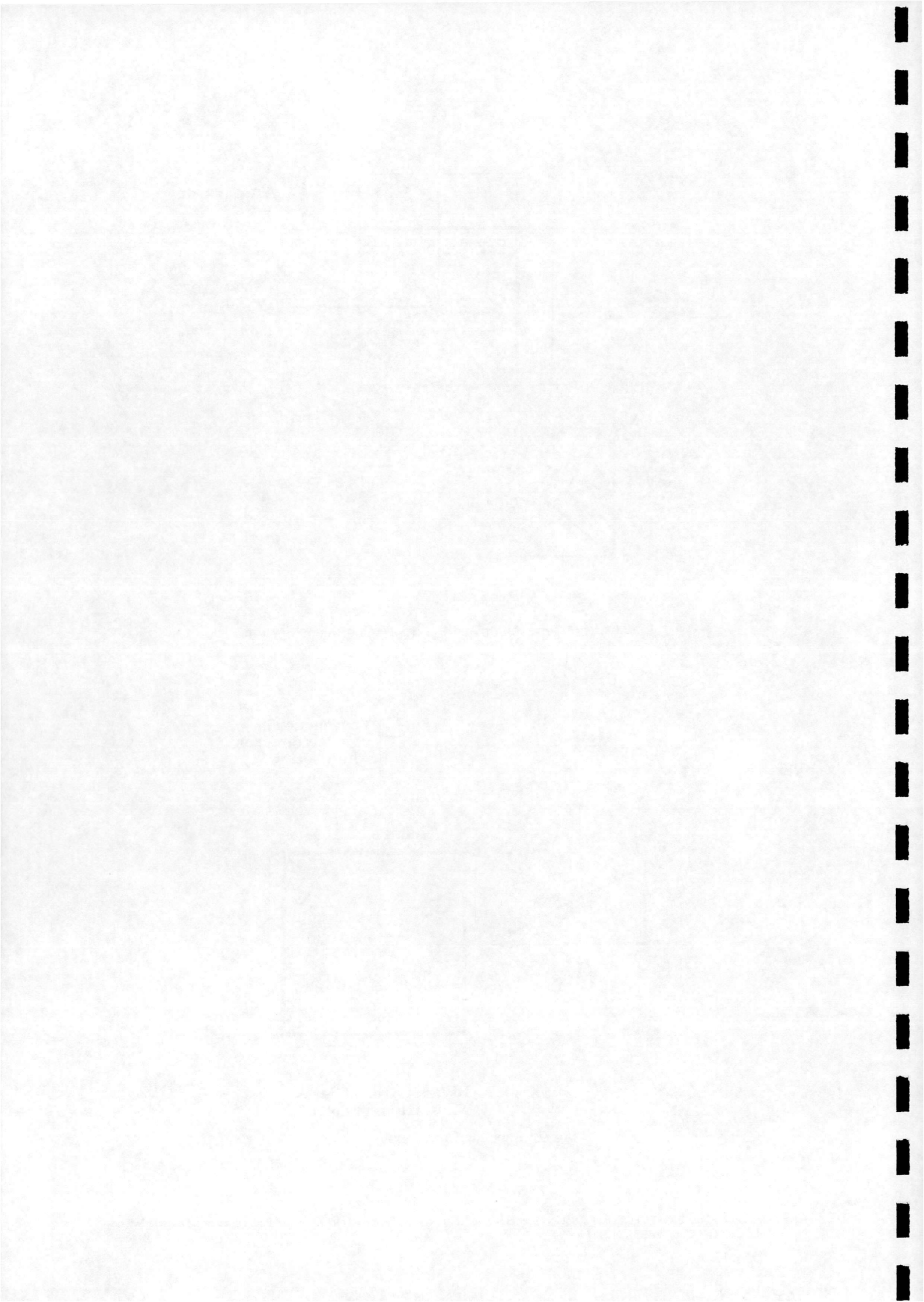
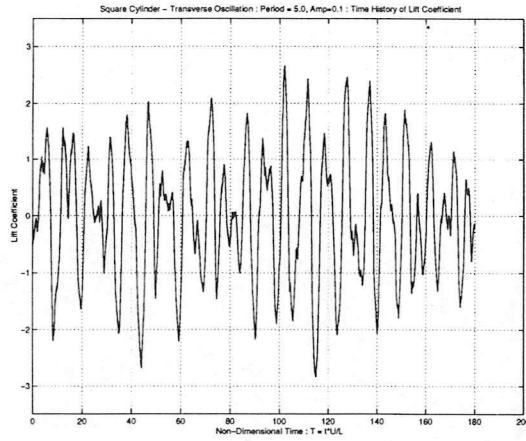
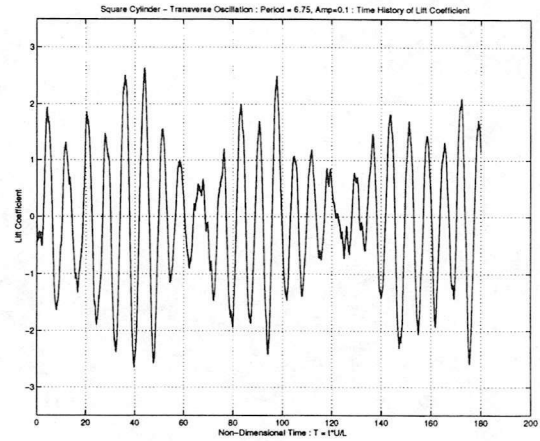


Fig. 2 - Labeling Conventions.

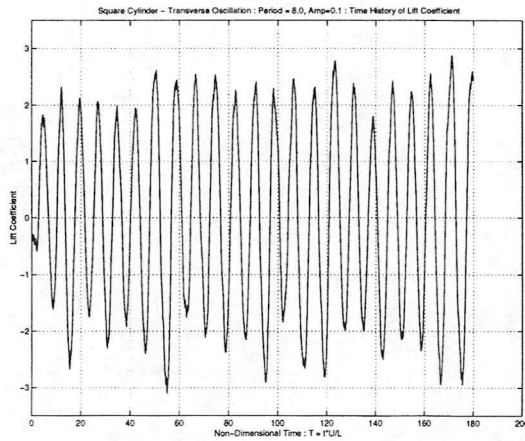




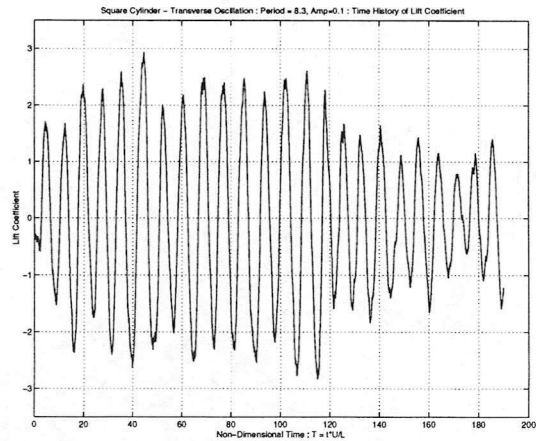
a) Reduced Velocity = 5.0.



b) Reduced Velocity = 6.75.

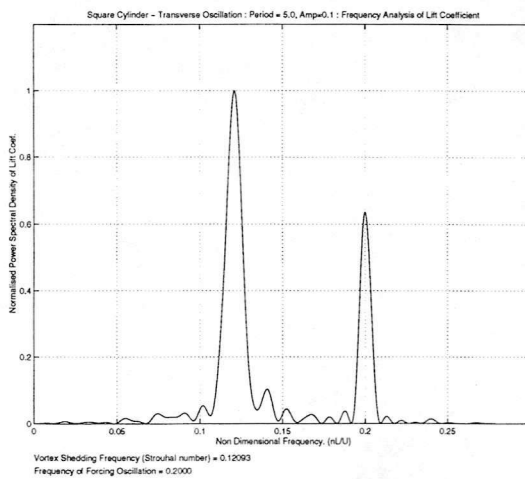


c) Reduced Velocity = 8.0.

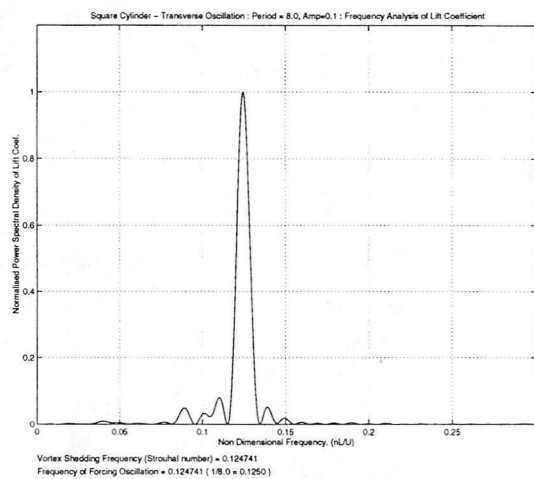


d) Reduced Velocity = 8.3.

Fig. 3 - Sample Lift Histories for Square Cylinder with Transverse Oscillation.

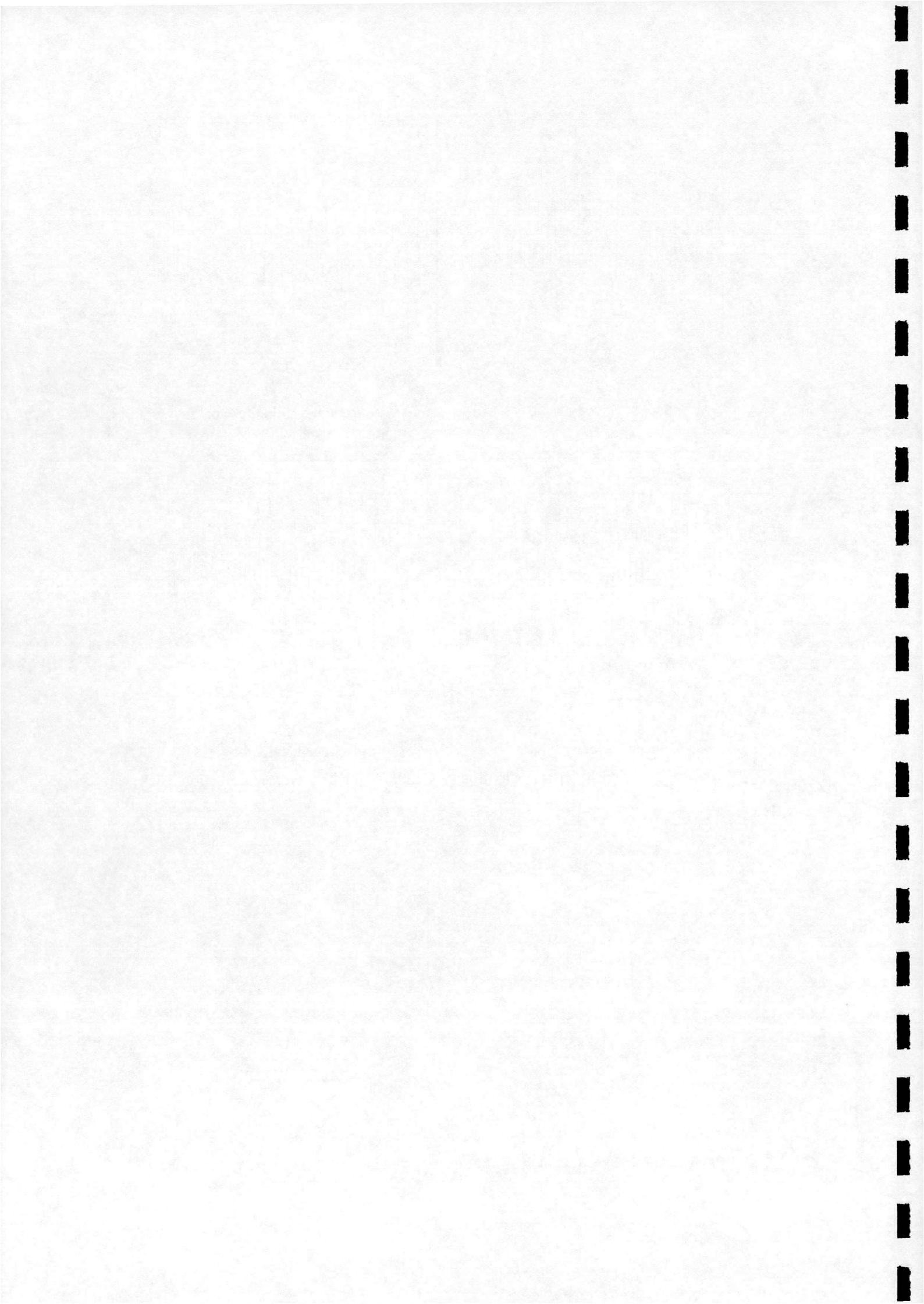


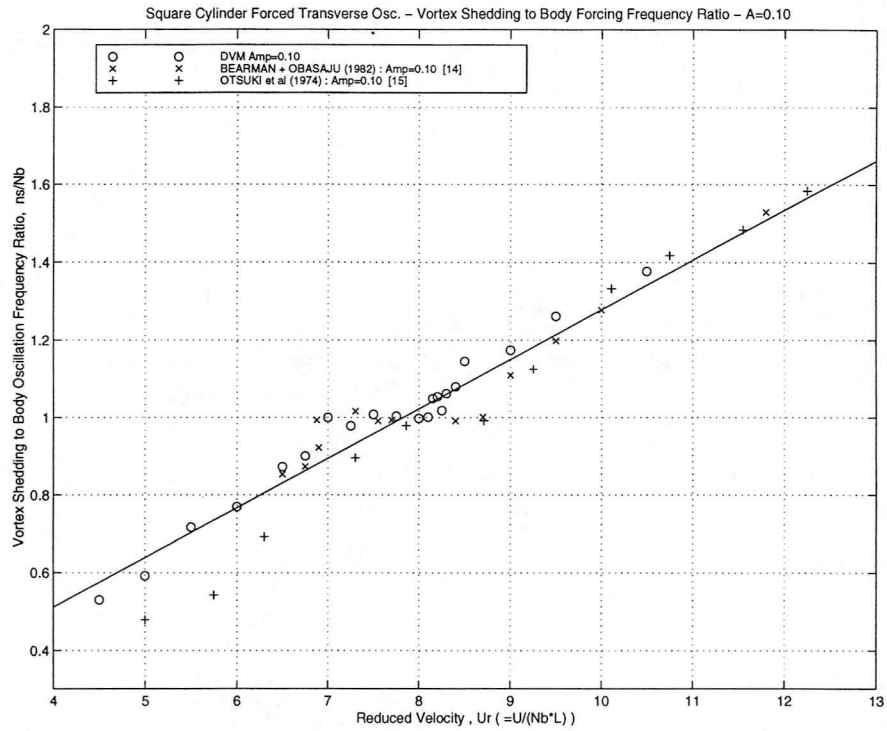
a) Reduced Velocity = 5.0 (Below Lock-in).



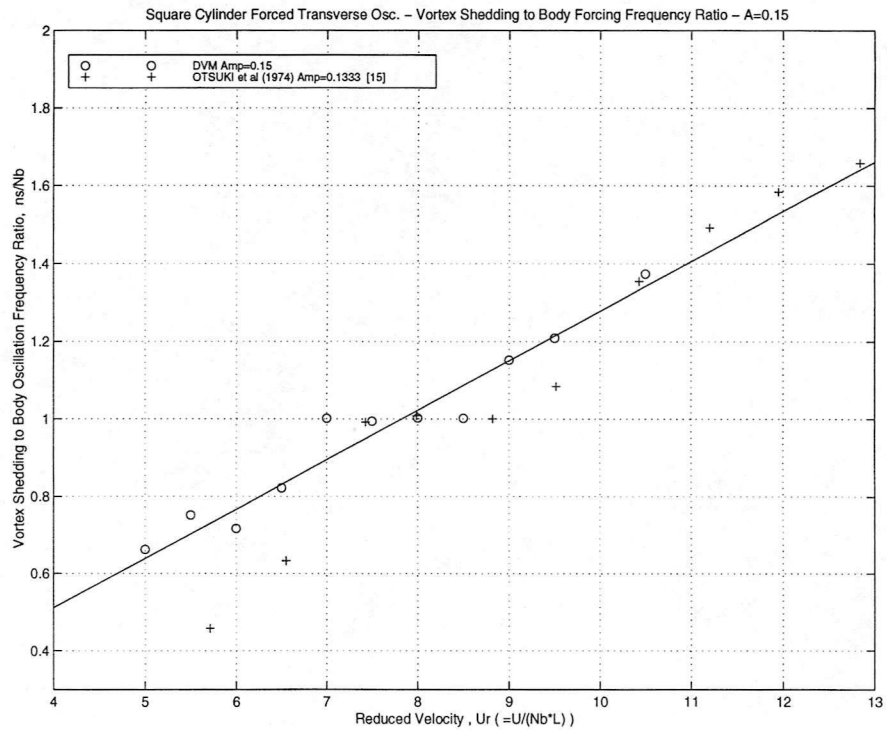
b) Reduced Velocity = 8.0 (Lock-in).

Fig. 4 - Sample Spectral Analysis for Square Cylinder with Transverse Oscillation.



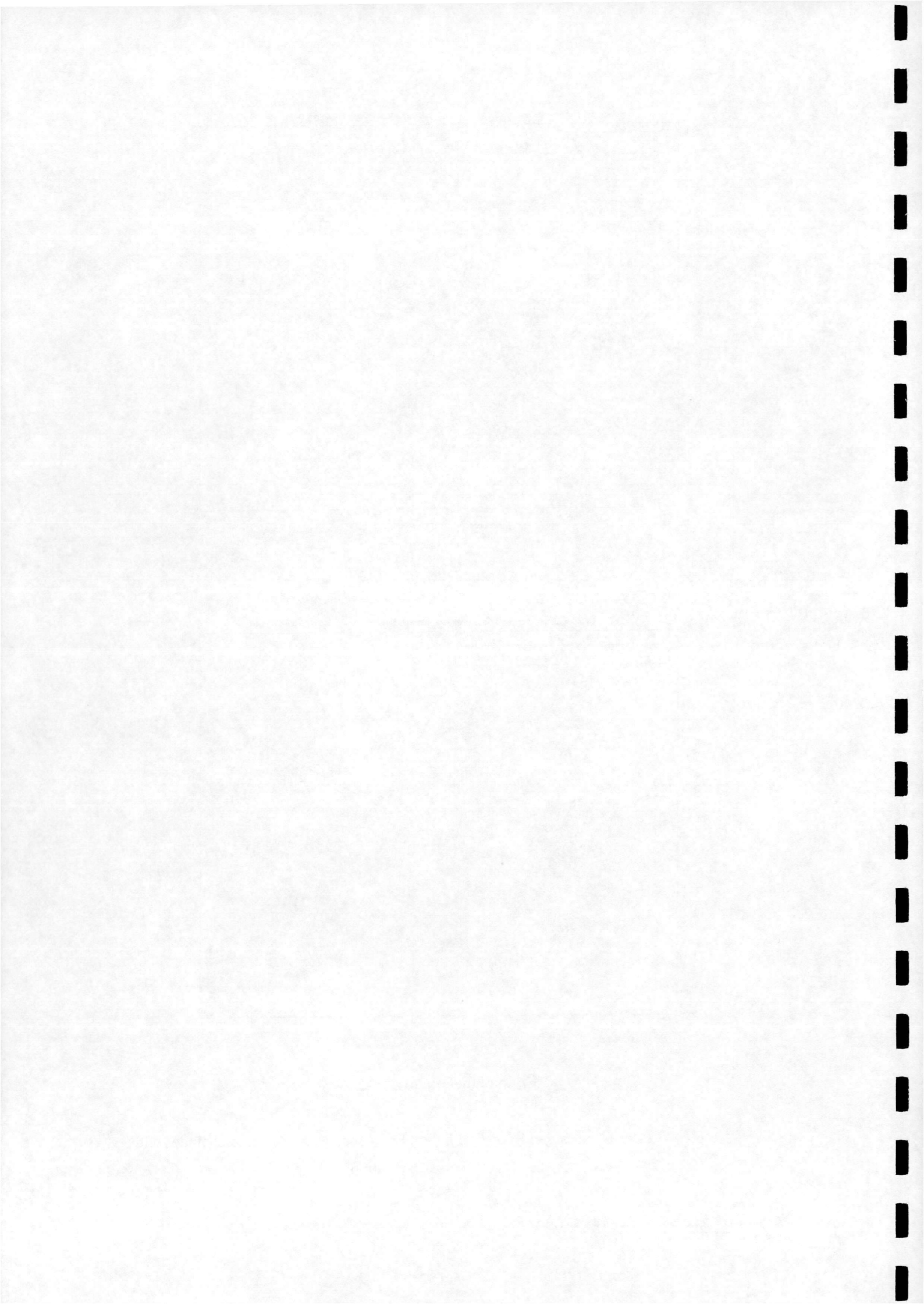


a) Amplitude Ratio = 0.10



b) Amplitude Ratio = 0.15

Fig. 5 - Vortex Shedding to Body Oscillation Frequency Ratio : Square Cylinder with Transverse Oscillation.



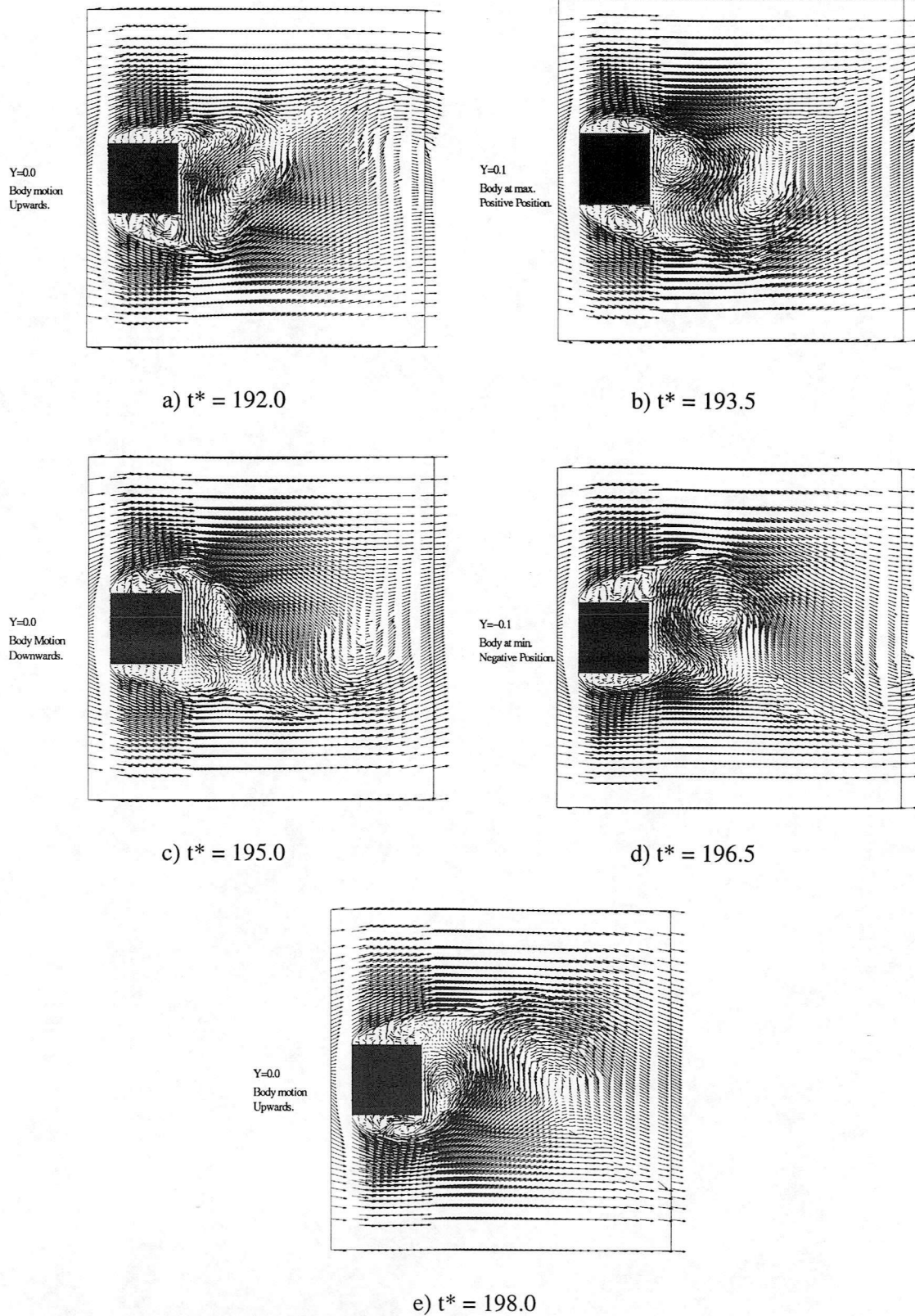
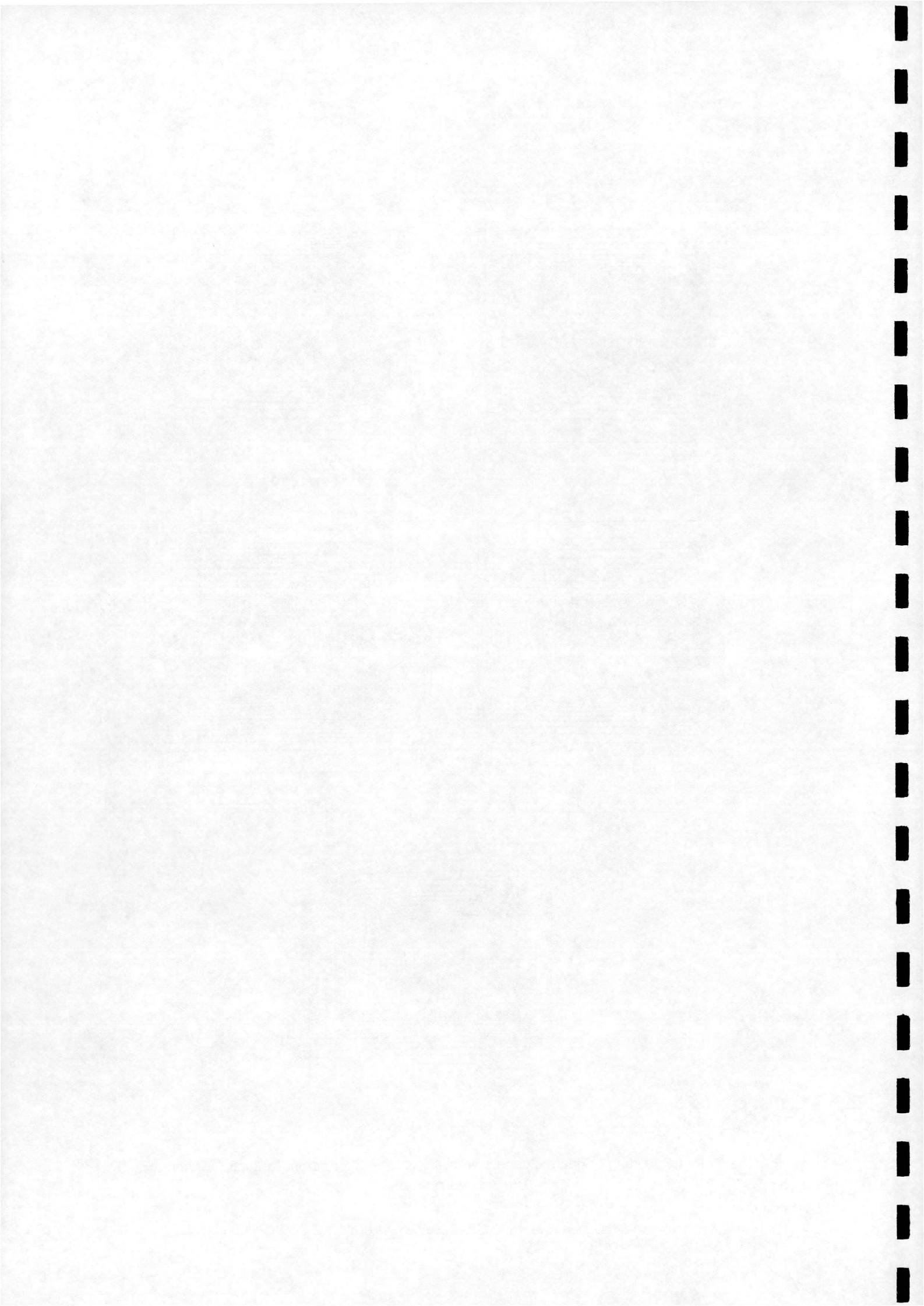


Fig. 6 - Velocity Vectors : Square Cylinder with Transverse Oscillation, Reduced Velocity = 6.0 (Below Lock-in).



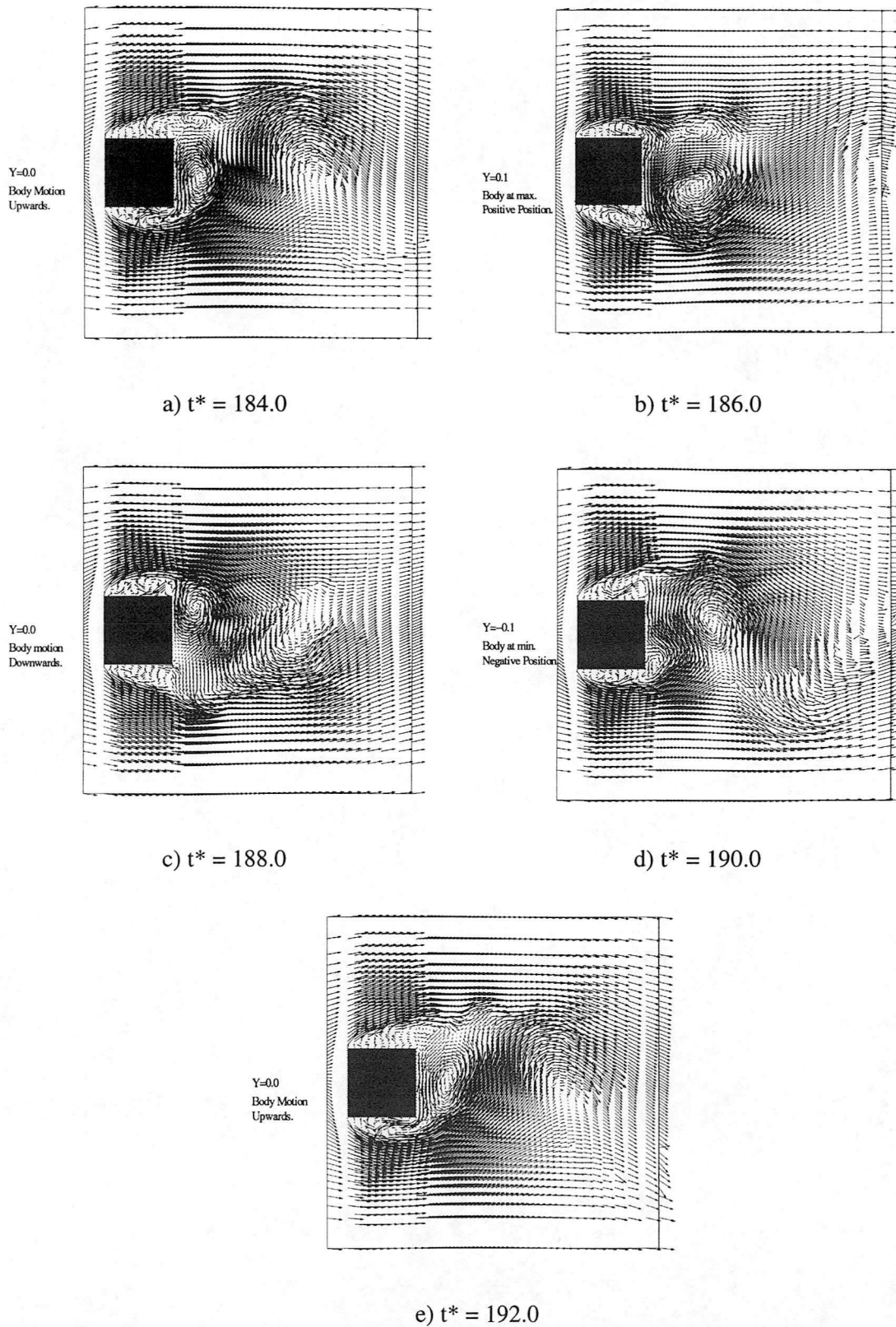
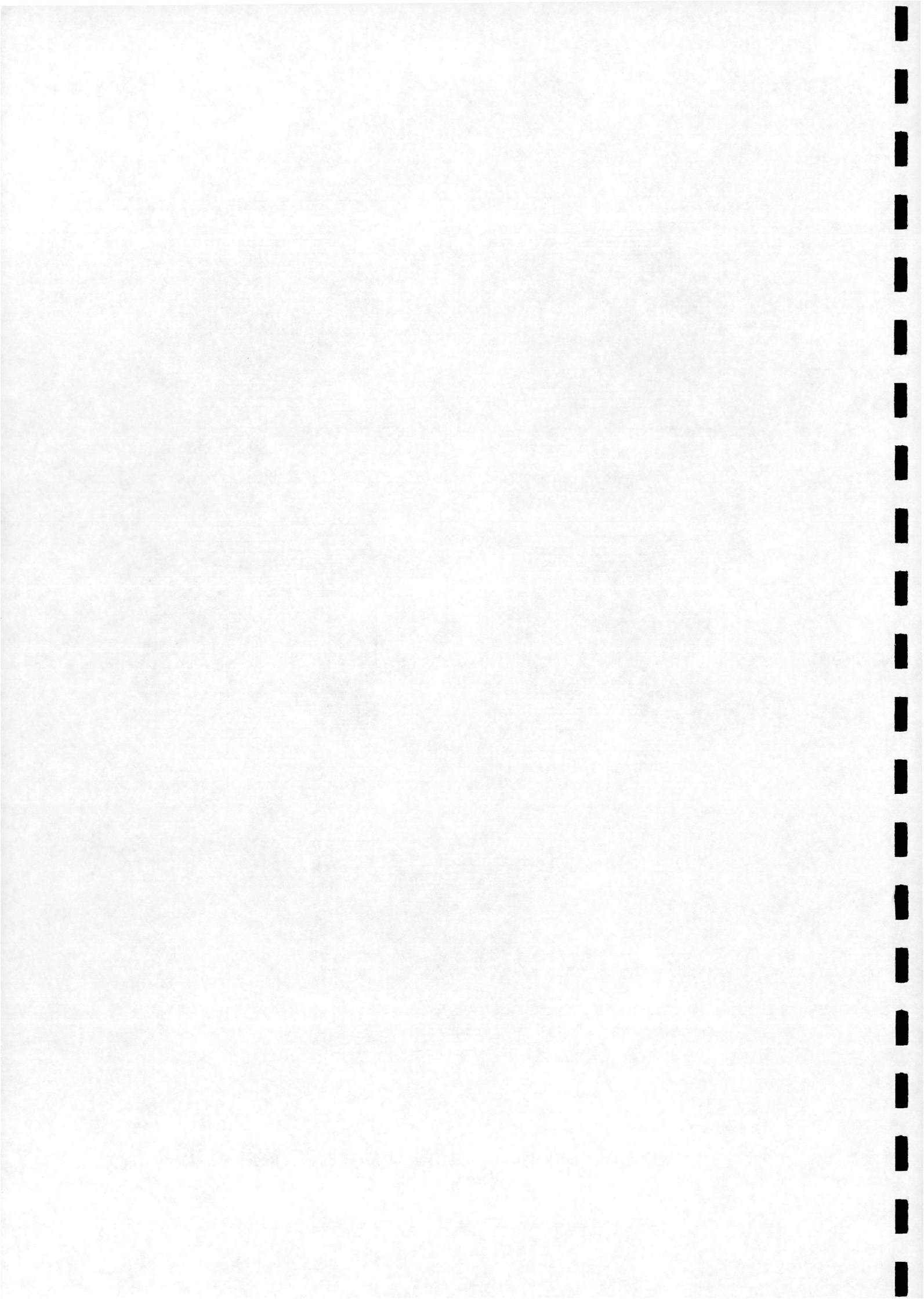
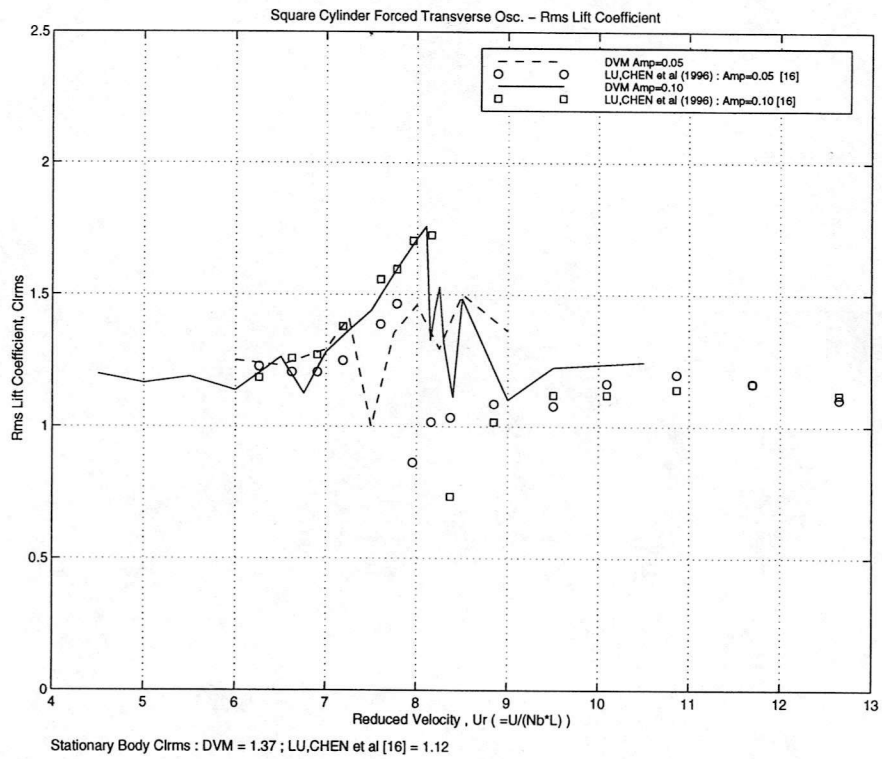
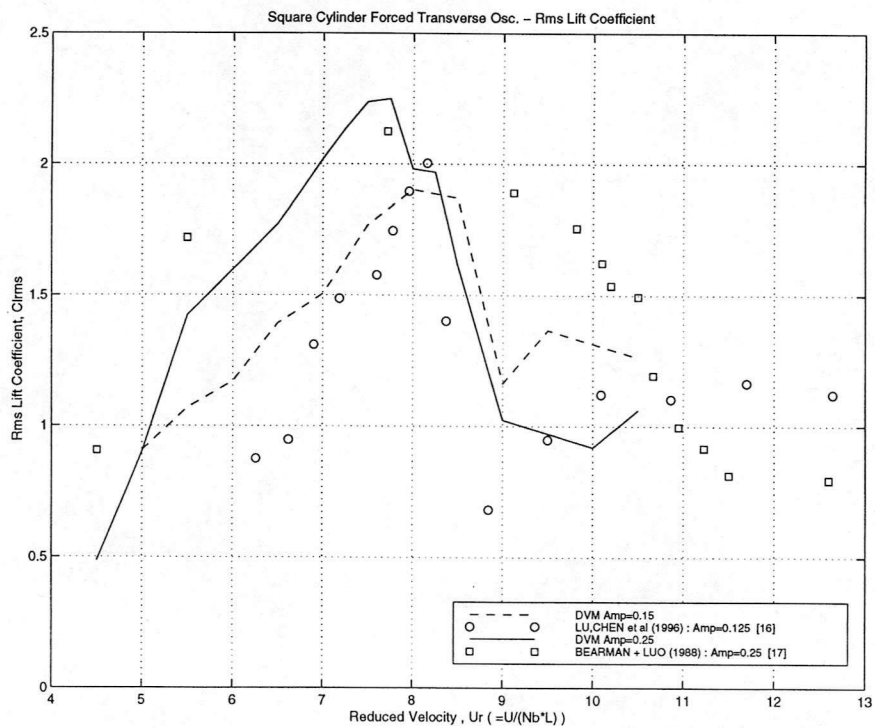


Fig. 7 - Velocity Vectors : Square Cylinder with Transverse Oscillation, Reduced Velocity = 8.0 (Vortex Lock-in).



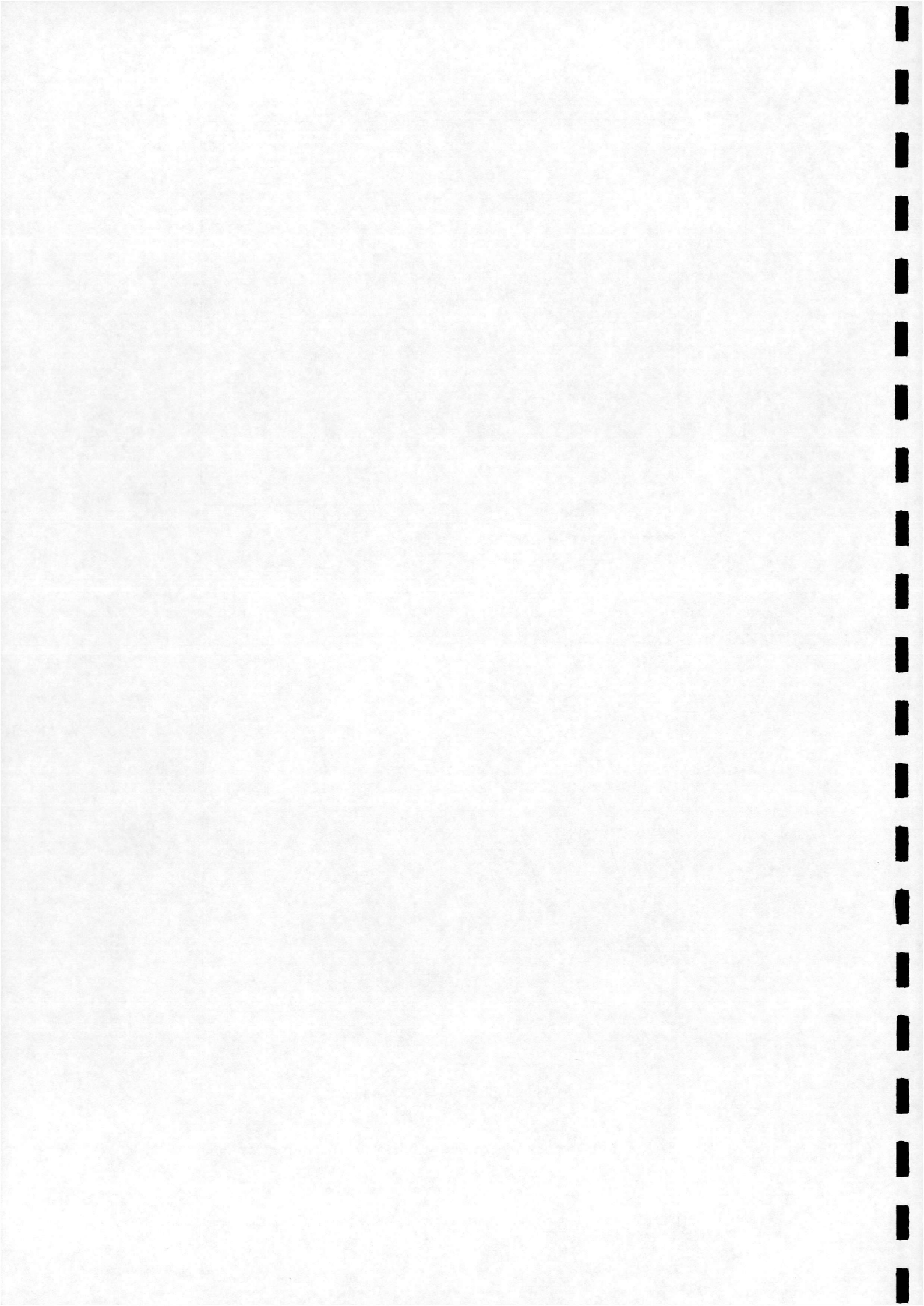


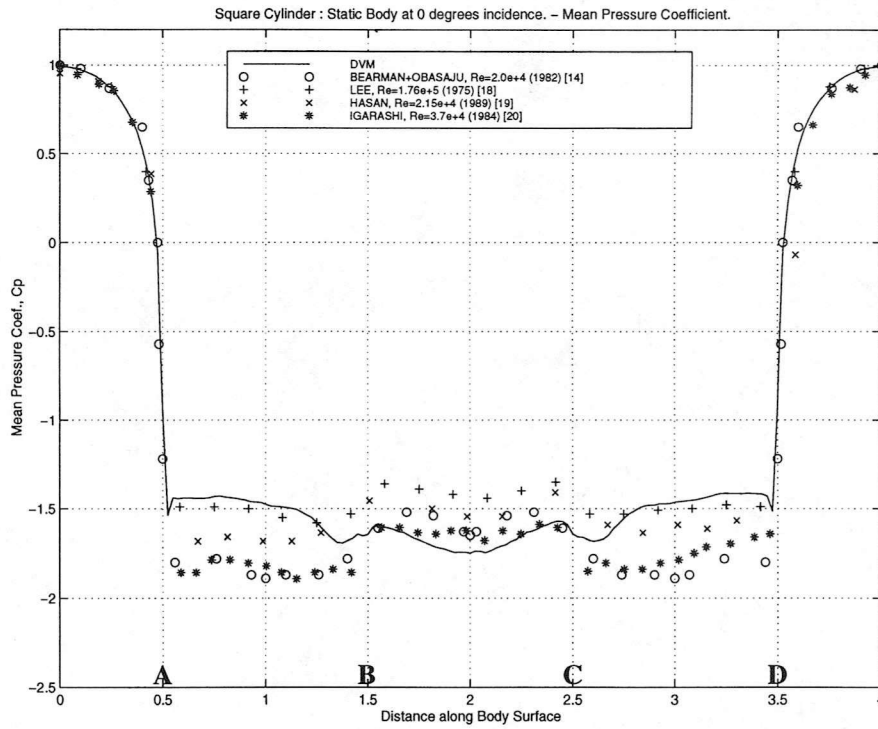
a) Amplitude Ratio = 0.05 and 0.10.



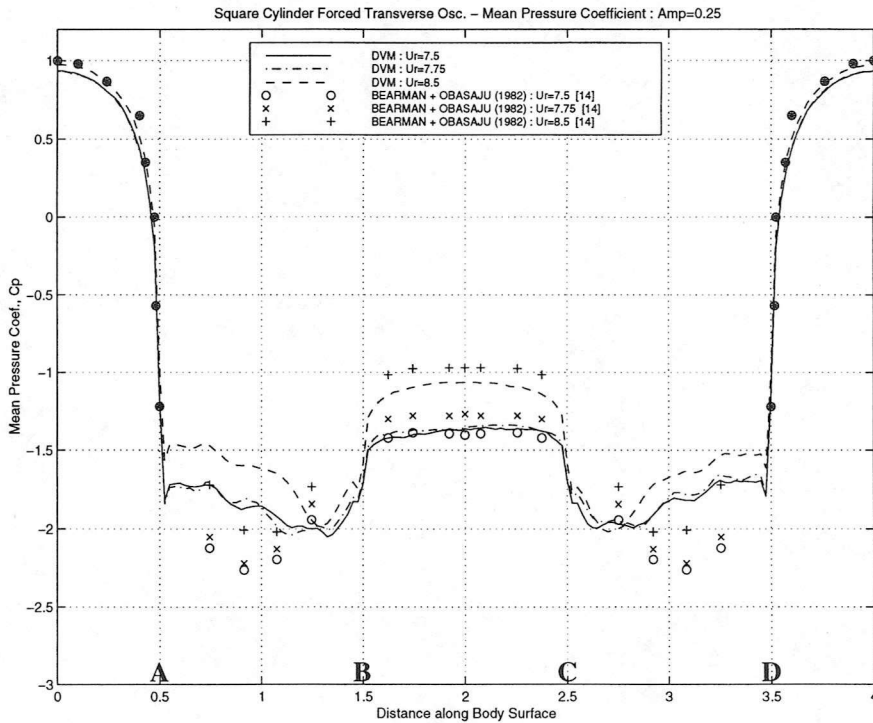
b) Amplitude Ratio = 0.15 and 0.25.

Fig. 8 - Rms Lift Coefficient : Square Cylinder with Transverse Oscillation.



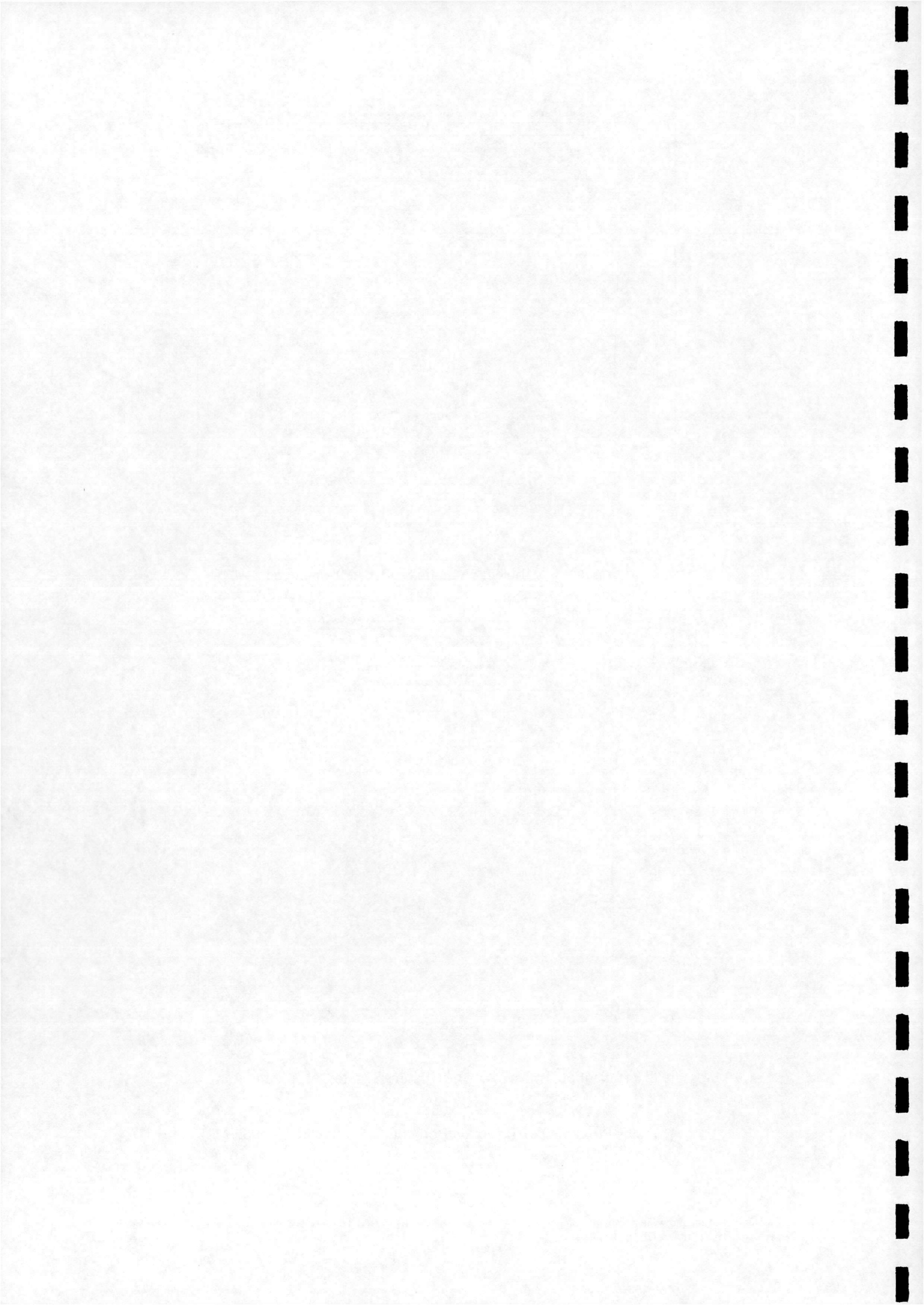


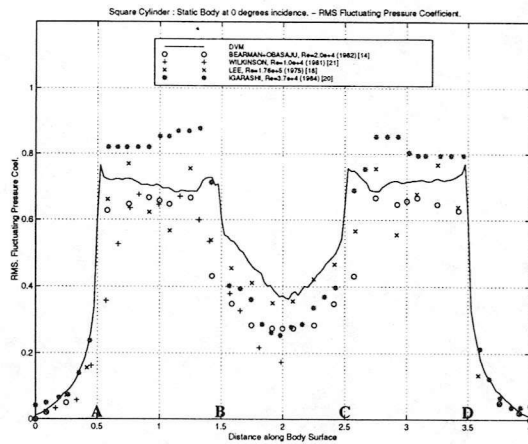
a) Pressure Coefficient on Static Square at 0° Incidence.



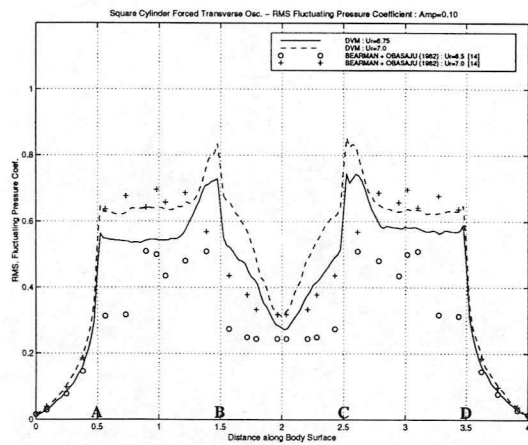
b) Pressure Coefficient on Transversely Oscillating Square : Amplitude Ratio = 0.25.

Fig. 9 - Pressure Coefficient on Body Surface : Square Cylinder.

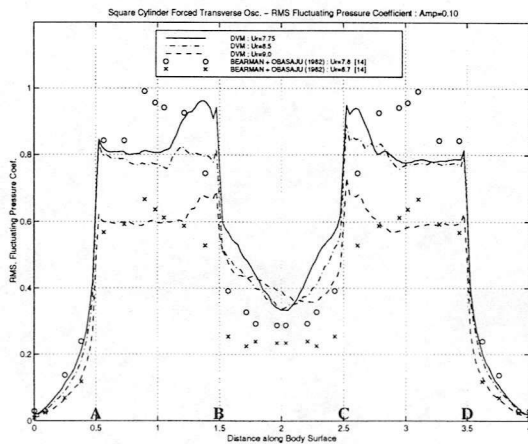




a) Rms Pressure Coefficient on Static Square at 0° Incidence.

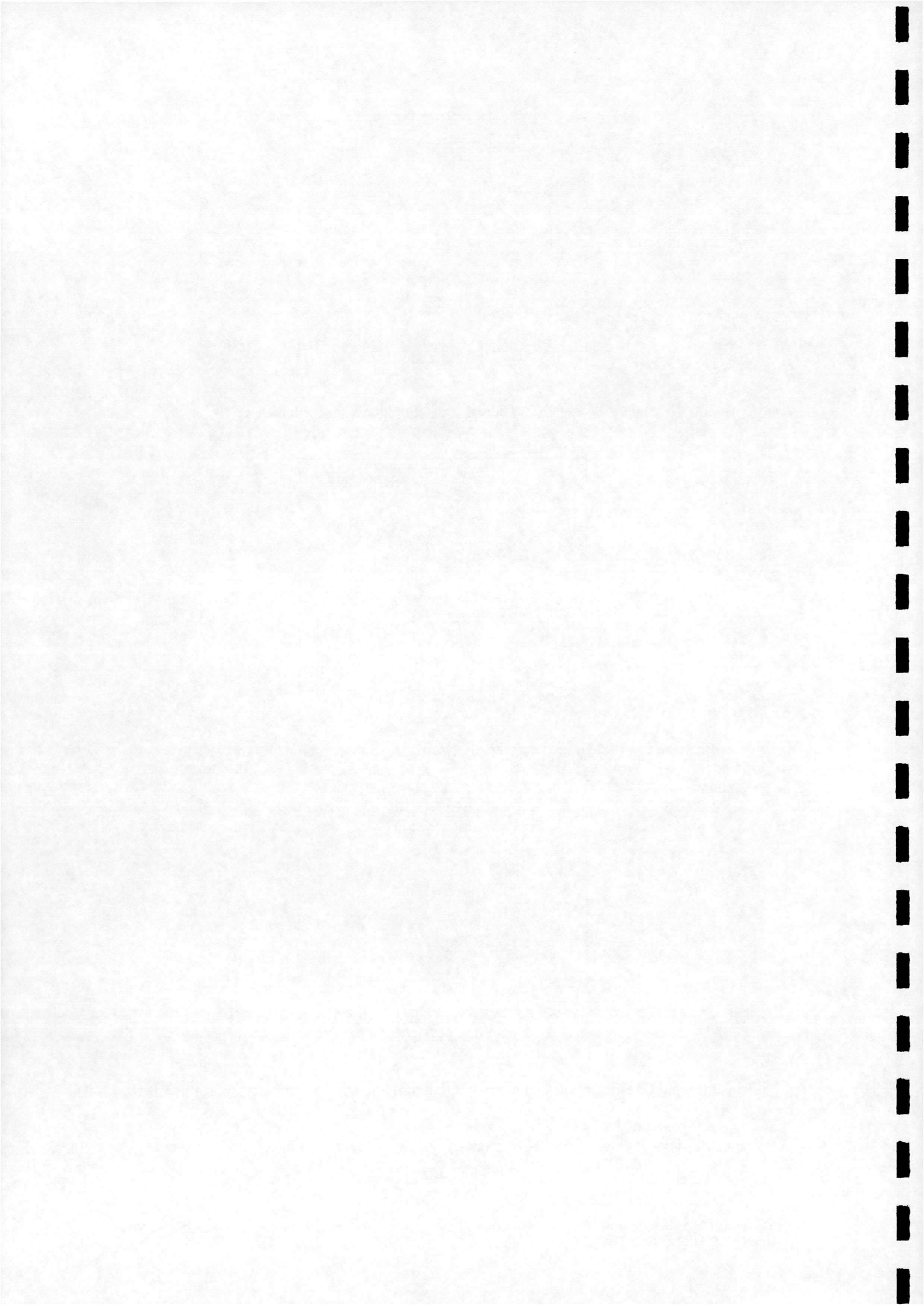


b) Rms Pressure Coefficient on Transversely Oscillating Square : Low U_r , Amp. Ratio = 0.10.



c) Rms Pressure Coefficient on Transversely Oscillating Square : High U_r , Amp. Ratio = 0.10.

Fig. 10 - Rms Pressure Coefficient on Body Surface : Square Cylinder with Transverse Oscillation.



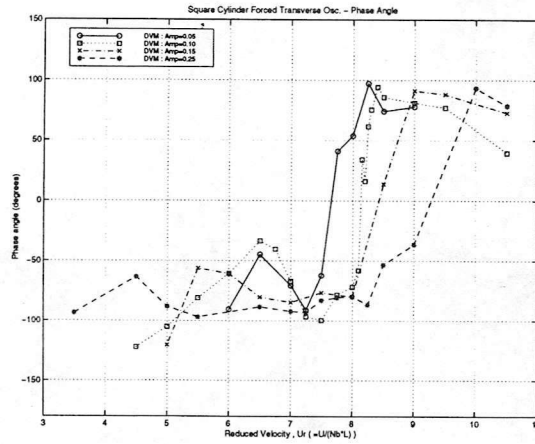
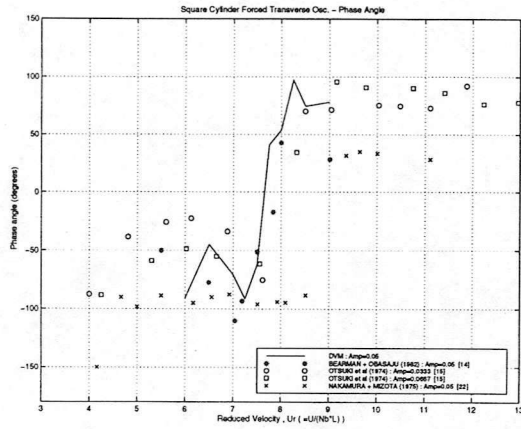
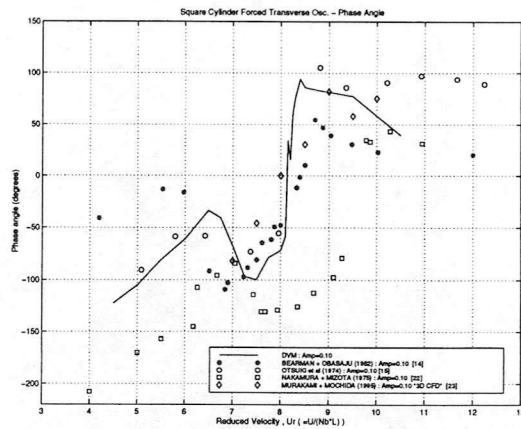


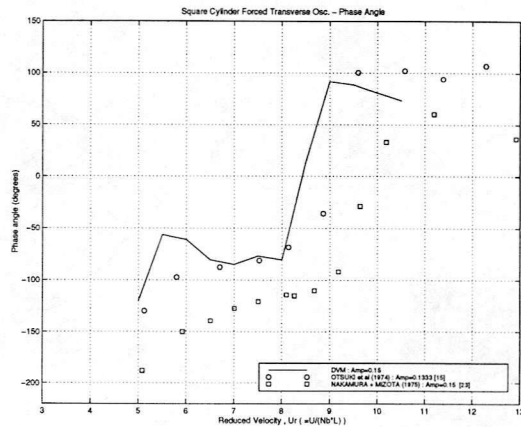
Fig. 11 - Phase Angle : Calculated Results from DVM.



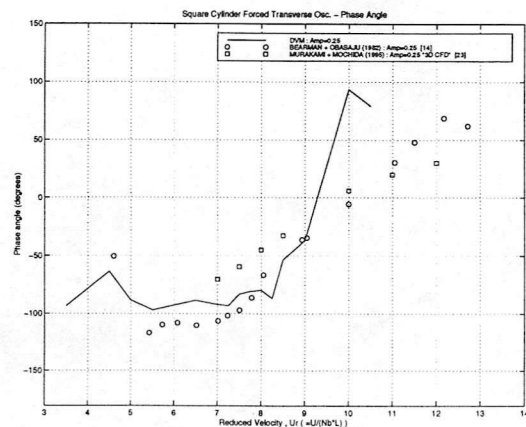
a) Phase Angle : Amp. Ratio = 0.05



b) Phase Angle : Amp. Ratio = 0.10

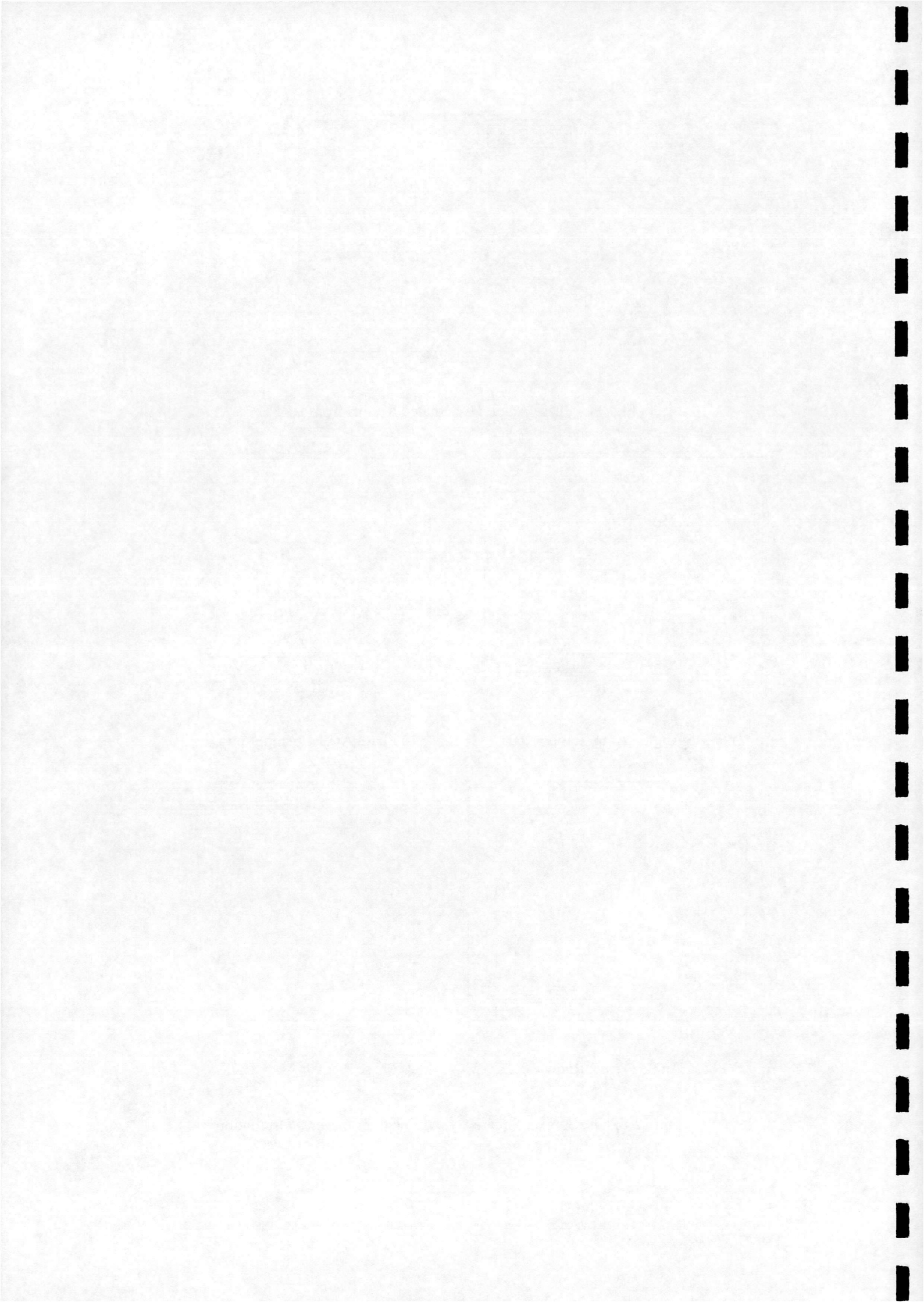


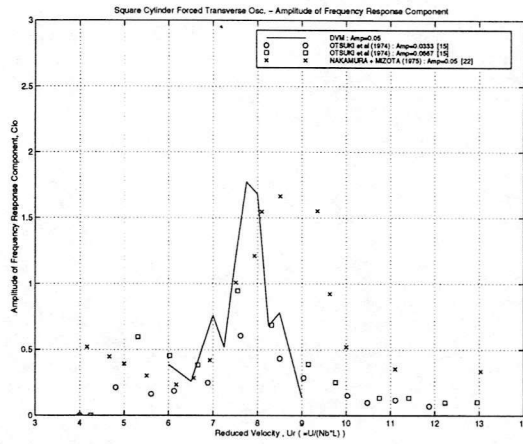
c) Phase Angle : Amp. Ratio = 0.15



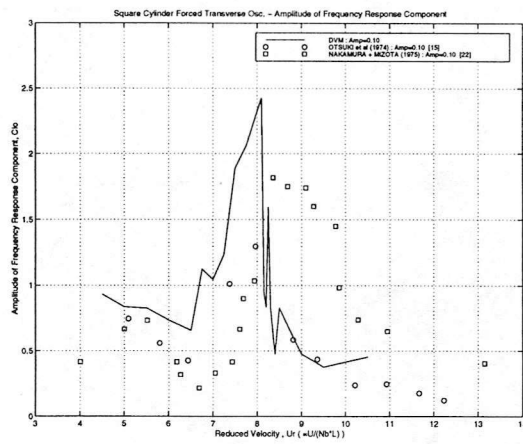
d) Phase Angle : Amp. Ratio = 0.25

Fig. 12 - Phase Angle : Square Cylinder with Transverse Oscillation.

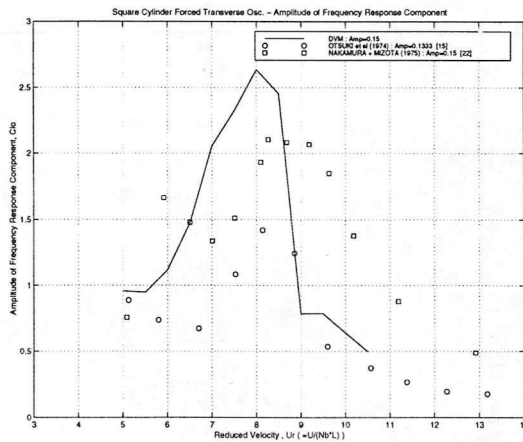




a) Amplitude Ratio = 0.05.

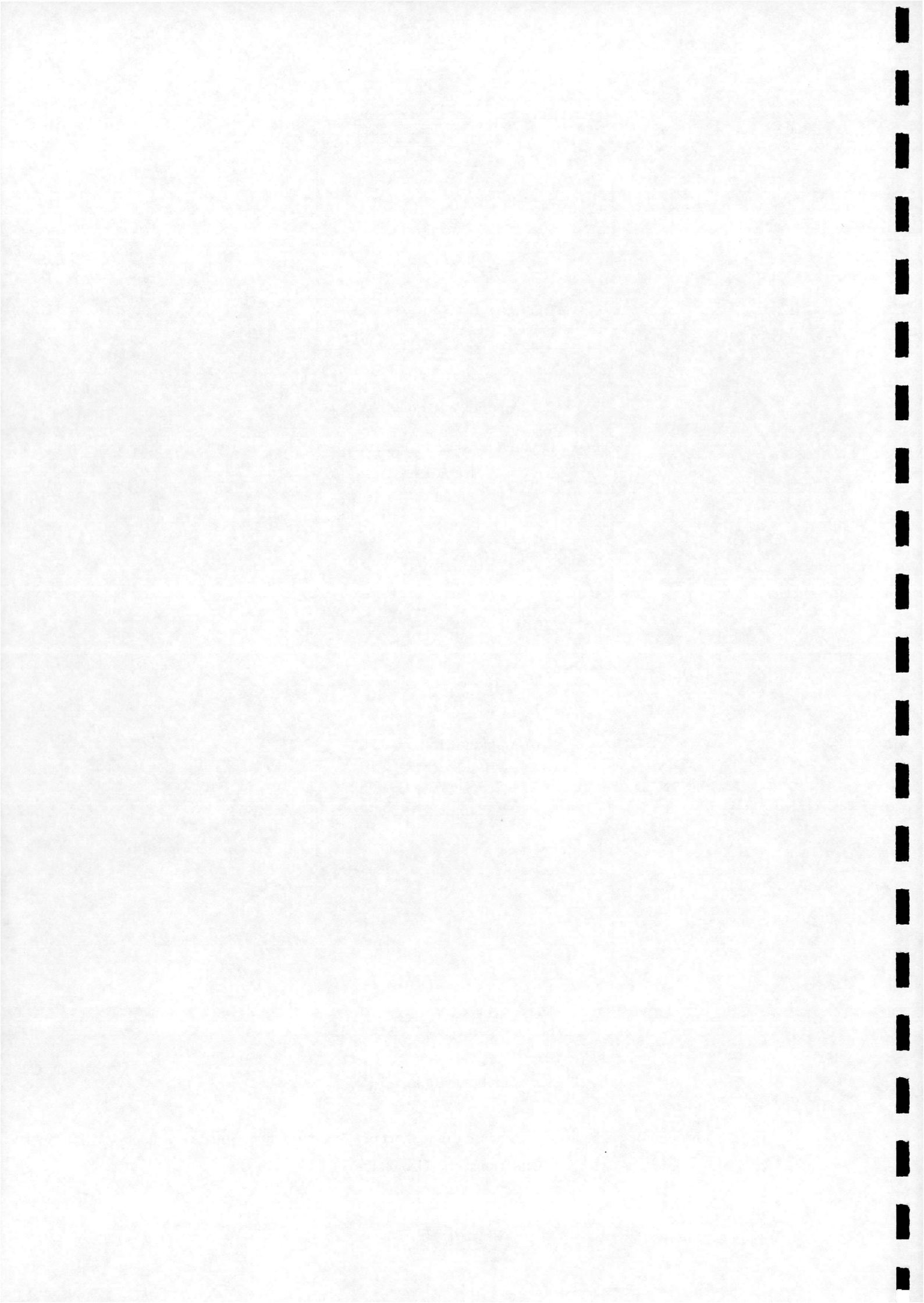


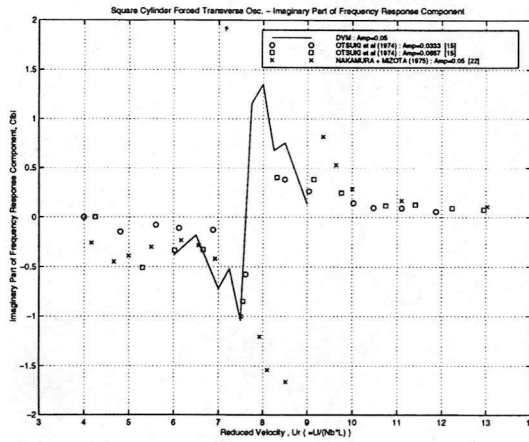
b) Amplitude Ratio = 0.10.



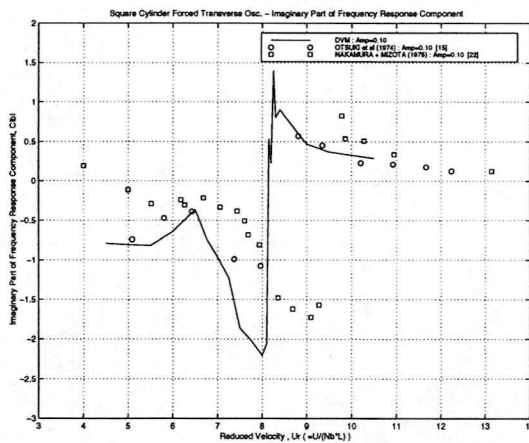
c) Amplitude Ratio = 0.15.

Fig. 13 - Amplitude of Frequency Response Component of Lift Coefficient : Square Cylinder with Transverse Oscillation.

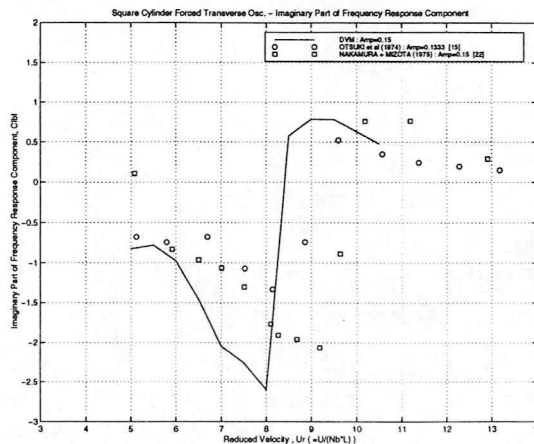




a) Amplitude Ratio = 0.05.



b) Amplitude Ratio = 0.10.



c) Amplitude Ratio = 0.15.

Fig. 14 - Imaginary Part of Frequency Response Component of Lift Coefficient : Square Cylinder with Transverse Oscillation.

